

This is a repository copy of *miR-132 suppresses transcription of ribosomal proteins to promote protective Th1 immunity*.

White Rose Research Online URL for this paper:

<https://eprints.whiterose.ac.uk/143286/>

Version: Accepted Version

Article:

Hewitson, James Philip orcid.org/0000-0002-3265-6763, Shah, Kunal M, Brown, Najmeeyah et al. (6 more authors) (2019) miR-132 suppresses transcription of ribosomal proteins to promote protective Th1 immunity. EMBO Reports. e46620. ISSN 1469-221X

<https://doi.org/10.15252/embr.201846620>

Reuse

Items deposited in White Rose Research Online are protected by copyright, with all rights reserved unless indicated otherwise. They may be downloaded and/or printed for private study, or other acts as permitted by national copyright laws. The publisher or other rights holders may allow further reproduction and re-use of the full text version. This is indicated by the licence information on the White Rose Research Online record for the item.

Takedown

If you consider content in White Rose Research Online to be in breach of UK law, please notify us by emailing eprints@whiterose.ac.uk including the URL of the record and the reason for the withdrawal request.

- The miR-132/212 cluster controls ribosomal protein expression through directly targeting two transcriptional co-activators, BTAf1 and p300.

- *Leishmania donovani*-infected *miR-132/212*^{-/-} mice display increased IL-10 and reduced IFN γ protein expression in Th1 cells, reduced hepatosplenomegaly, and increased parasite burdens.

ABSTRACT

Determining the mechanisms that distinguish protective immunity from pathological chronic inflammation remains a fundamental challenge. miR-132 has been shown to play largely immunoregulatory roles in immunity, however its role in CD4⁺ T cell function is poorly understood. Here, we show that CD4⁺ T cells express high levels of miR-132 and that T cell activation leads to miR-132 up-regulation. The transcriptomic hallmark of splenic CD4⁺ T cells lacking the miR-132/212 cluster during chronic infection is an increase in mRNAs levels of ribosomal protein (RP) genes. BTAf1, a co-factor of B-TFIID and novel miR-132/212-3p target, and p300 contribute towards miR-132/212-mediated regulation of RP transcription. Following infection with *Leishmania donovani* *miR-132*^{-/-} CD4⁺ T cells display enhanced expression of IL-10 and decreased IFN γ . This is associated with reduced hepatosplenomegaly and enhanced pathogen load. The enhanced IL-10 expression in *miR-132*^{-/-} Th1 cells is recapitulated *in vitro* following treatment with phenylephrine, a drug reported to promote ribosome synthesis. Our results uncover that miR-132/212-mediated regulation of RP expression is critical for optimal CD4⁺ T cell activation and protective immunity against pathogens.

INTRODUCTION

54 MicroRNAs (miRNAs) are endogenous small silencing RNAs with fundamental roles in
55 the immune system [1]. In this context, miR-132-3p (miR-132) is derived from the miR-
56 212/132 cluster and has emerged as key regulator of immune cell development and
57 function [1, 2]. During innate immune activation, miR-132 is induced upon and plays a
58 crucial role in the transcriptional response to pathogenic challenge [3-6]. We have
59 previously shown that miR-132 is induced in a dose-dependent manner upon viral
60 infection and suppresses the innate antiviral immune response by down-regulating
61 expression of p300 (official symbol EP300), a necessary co-activator for several key
62 transcription factors [3]. Furthermore, miR-132 has been shown to be critical for normal
63 haematopoiesis and B cell development and function through suppression of FOXO3
64 and SOX4, respectively [7, 8], whereas the miR-212/132 cluster has also been
65 implicated in Th17 responses [9]. miR-132 is also up-regulated in a model of
66 inflammation-induced cellular transformation [10], plays a key role inflammation during
67 wound healing [11], is induced *in vivo* following infection by *Toxoplasma gondii* [12], and
68 regulates macrophage activation following *Mycobacterium tuberculosis* infection [13].
69 Although the above studies have provided strong support for the role of miR-132 in the
70 immune system, they have predominantly focused on acute inflammation or infection
71 models whereas the role of miR-132 in models of pathogen-induced chronic
72 inflammation remains poorly explored. For example, we have limited knowledge on
73 whether miR-132 is dispensable for T cell-mediated immunity.

74

75 Here we show that miR-132 is induced upon activation of CD4⁺ T cells *in vitro* and *in*
76 *vivo* during infection of mice with *Leishmania donovani* (*L. donovani*). Using fully *miR*-
77 *212/132*-deficient mice [14] (hereafter referred to as *miR-132*^{-/-} mice), we show that the
78 transcriptomic hallmark of miR-132 deficiency in CD4⁺ T cells isolated from chronically
79 infected spleens is an increase in mRNAs levels of ribosomal protein (RP) genes.
80 Similarly, miR-132 controls RP gene mRNA levels during *in vitro* activation of CD4⁺ T
81 cells. Enhanced ribosome biosynthesis during *in vitro* CD4⁺ T cell activation is thought

82 to be necessary for accommodating the needs for cytokine production in activated cells
83 [15]. However, the *in vivo* relevance of this phenomenon and the molecular drivers
84 underpinning it remain largely unexplored. Notably, miR-132 over-expression
85 suppresses RP gene expression and protein synthesis rates in mouse embryonic
86 fibroblasts (MEFs). Regulation of RP gene expression is mediated by miR-132-mediated
87 silencing of proteins involved in transcription including p300 and BTAF1, which we
88 identified here as a novel miR-132 target. *In vivo*, *miR-132^{-/-}* CD4⁺ T cells from
89 chronically infected mice express higher levels of IL-10 and lower levels of IFN γ when
90 compared to WT cells. This functional impairment correlates with reduced
91 immunopathology and increased pathogen burdens in *L. donovani*-infected *miR-132^{-/-}*
92 mice. *In vitro*, activated *miR-132^{-/-}* CD4⁺ T cells treated with the hypertrophic factor
93 phenylephrine (PE) also demonstrate enhanced IL-10 expression. Overall, the above
94 demonstrate that miR-132 is a necessary and sufficient regulator of RP gene expression
95 through targeting core transcriptional regulators and that this mechanism contributes
96 towards optimal CD4⁺ T cell activation and protective immunity.

97

98 **RESULTS AND DISCUSSION**

99 **miR-132 is up-regulated during CD4⁺ T cell activation**

100 We first determined whether miR-212/132 levels were regulated following stimulation of
101 naïve (CD62L⁺ CD44⁻) CD4 T cells with anti-CD3 and anti-CD28 antibodies, and found
102 strong miR-132-3p and -212-3p up-regulation that peaked at day 1 (18hrs) (**Fig. 1A**; ~20
103 and ~30 fold increase compared to unstimulated cells) and remained elevated for at
104 least 3 days. Expression of the *miR-212/132* primary transcript is CREB-dependent [16],
105 and as expected [17], TCR stimulation induced strong CREB phosphorylation within 2-
106 4 hours, and this was sustained for 3 days (**Fig. EV1A**). Whilst miR-146-5p showed little
107 change following T cell activation, miR-155-5p was strongly up-regulated for sustained
108 periods, whereas miR-16-5p levels declined (**Fig. 1A**). miR-132-3p and miR-212-3p up-

regulation appeared to be a common feature in activated CD4⁺ T cells, and occurred regardless of T cell polarisation phenotype (Th0, Th1 and Th2; **Fig. EV1B**).

To investigate the role of miR-212/132 in the development of inflammation and protective immune responses *in vivo*, we studied its expression in naïve and infected C57BL/6 WT mice with *L. donovani* amastigotes. This infection model allows the study of host-pathogen interactions [18], during which infection occurs in the liver, spleen, and bone marrow. We sorted splenic lymphocytes and found that CD4⁺ T cells express higher miR-132-3p levels than CD8⁺ T cells or B cells (**Fig. 1B**). Furthermore, *L. donovani* infection resulted in miR-132-3p up-regulation in CD4⁺ T cells. The extent of this up-regulation was similar to that observed for miRNAs previously reported to be involved in T cell responses such as 146-5p and 155-5p [19, 20]. Combining these results with previous findings demonstrating miR-132 induction downstream of TLR [3-5] and the B cell receptor [7] establishes miR-132 induction as a hallmark of innate and adaptive immune activation. Of note, miR-132 up-regulation has also been observed in studies using human bulk CD4⁺ and CD8⁺ T cell populations where it was amongst the most prominent up-regulated miRNAs [21].

miR-212/132-deficiency is associated with global up-regulation of ribosomal protein genes in CD4⁺ T cells from chronically infected spleens.

To gain a molecular understanding of the function of the miR-132/212 cluster in CD4⁺ T cells *in vivo*, we performed RNAseq analysis on biological replicates of sorted splenic CD4⁺ T cells from *L. donovani*-infected WT and *miR-132*^{-/-} mice. Of the more than 14,000 genes that were detectable in CD4⁺ T cells, similar numbers showed up- or down-regulation by >50% in *miR-132*^{-/-} compared to WT cells (**Fig. 1C**; 10.3% up and 10.6% down). However, of the 1290 significantly differently expressed genes (9% of total), approximately 2/3 (850) were up-regulated in *miR-132*^{-/-} cells compared to WT and only 1/3 (440) down-regulated. Pathway analysis of genes significantly up-regulated in *miR-132*^{-/-} mice (p<0.05, >50% regulation) using the Gene Set Enrichment Analysis [22] and

STRING tools [23] revealed that a cluster of RP genes was significantly over-represented amongst genes upregulated in *miR-132*^{-/-} CD4⁺ T cells (**Fig. 1D and 1E**). This up-regulation was evident for both small (RPS) and large (RPL) subunits protein genes and even pseudogene transcripts (**Fig. 1F**). These results were further validated by qPCR, showing an increase in all tested RP genes, reaching statistical significance for RPL27, RPS10 and RPL14-ps1 (**Fig. 1G**). To explore the significance of the observed increase in RP gene expression in *miR-132*^{-/-} CD4⁺ T cells, we analysed published transcriptional profiles of *in vitro* generated Th1 and Th2 cells [24] and found that CD4⁺ T cell activation results in a statistically significant shift towards global up-regulation of RP gene levels (**Fig. 1H and Fig. EV1C**). Taken together with previous reports demonstrating that activation of ribosome biosynthesis is associated with activation of CD8⁺ T cells [25] and production of cytokines by CD4⁺ T cells *in vitro* [15], our findings suggested that the observed RP gene up-regulation in *miR-132*^{-/-} CD4⁺ T cells was a signature of enhanced activation.

The B-TFIID cofactor BTAF1 is a direct miR-132 target in CD4⁺ T cells.

To identify direct targets of the miR-132/212 cluster in CD4⁺ T cells, we performed RNAseq analysis of naïve CD4⁺ T cells from WT and *miR-132*^{-/-} mice prior to and following 1 day (18 hours) of *in vitro* TCR stimulation under Th1 conditions. We focussed on Th1 responses as these predominate in *L. donovani* infection and these cells displayed the highest levels of miR-132 expression (**Fig. EV1B**). Broadly similar numbers of transcripts were detected in unstimulated and stimulated T cells (12336 and 11140, respectively), with 5.0% (day 0 = 615) and 3.9% (day 1 = 432) showing significant differences between WT and *miR-132*^{-/-} mice (**Fig. 2A-B**). A much larger number of genes (44% WT, 54% *miR-132*^{-/-}) were differentially expressed when we compared naïve with activated T cells (**Fig. EV2A-B**). Of the genes that were significantly different between WT and *miR-132*^{-/-} mice ($p < 0.05$; 50% difference), 46% were up-regulated in *miR-132*^{-/-} at day 0, and this increased to 68% at day 1. At day 1, we observed that the

majority of predicted miR-132/212-3p targets were up-regulated (i.e. 51/75 =68% displayed a positive log2 fold change) in *miR-132^{-/-}* CD4⁺ T cells (**Fig. 2C-D**). Of note, a single predicted miR-132/212-3p target, BTA1, was up-regulated in both unstimulated and activated *miR-132^{-/-}* CD4⁺ T cells, as well as in CD4⁺ T cells from *L. donovani*-infected *miR-132^{-/-}* mice (**Fig. 2C-E, and Fig. EV2C**). Up-regulation of BTA1 was confirmed by qPCR (**Fig. 2F**). BTA1 protein expression was elevated in *miR-132^{-/-}* CD4⁺ T cells compared to WT cells, both before and after TCR stimulation (**Fig. 2G**). BTA1 contains a single 7mer-m8 site for miR-132/212-3p within its 3'UTR that is broadly conserved in mammals (**Fig. EV2D**). To assess whether BTA1 was a direct target of miR-132/212-3p, we transfected HeLa or 3T3 cells with luciferase reporter constructs preceded by ~1.5kb of *BTA1* 3'UTR (either WT or with miR-132/212-3p site mutated) in the presence of miR-132-3p or miR-212-3p mimics. This revealed that in the presence of miR-132-3p mimics, luciferase activity was significantly elevated following mutation of the miR-132/212 site in the 3'UTR (**Fig. 2H, Fig. EV2E**). A similar trend was observed in miR-212-3p transfected cells although this did not reach statistical significance. This demonstrated that miR-132 can directly interact with the predicted miR-132-binding site in the *BTA1* 3' UTR. We also searched for potential miR-132-5p and miR-212-5p targets that were altered in *miR-132^{-/-}* mice. Unlike miR-132-3p and miR-212-3p, these two miRNA differ in their seed sequence and so are predicted to have different mRNA targets (**Fig. EV2F**). Whilst several potential targets were significantly dysregulated in *miR-132^{-/-}* CD4⁺ cells, there was little overlap between those altered in unstimulated T cells, d1 activated T cells or those derived from d28 *L. donovani*-infection (**Fig. EV2G**). Only a single target, BACH2 (predicted 7mer-A1 target for both miR-212-5p and miR-132-5p), was up-regulated by >50% in all three T cell datasets, but this was only significant for *in vitro* d1 stimulated T cells and was highly variable in the other two conditions (**Fig. EV2H**).

Having observed an effect of miR-132 deletion on RP gene mRNA levels after chronic CD4⁺ T cell activation *in vivo* (**Fig. 1**), we tested whether we can observe a similar effect

in our dataset from the early stages of *in vitro* CD4⁺ T cell activation. Following 24h of *in vitro* activation of naïve CD4⁺ T cells, we observed that 40% of RP genes showed upregulation (positive log₂ fold change or LFC) in *WT* mice. This proportion was significantly increased to 61% in *miR-132*^{-/-} mice (P = 0.011) (**Fig. EV2I**). Furthermore, the vast majority of RP genes (81%) demonstrated a higher LFC (indicating stronger up-regulation or weaker downregulation) upon activation of *miR-132*^{-/-} CD4⁺ T cells compared to WT cells (**Fig. EV2J**).

p300 and BTAF1 contribute to miR-132-mediated suppression of ribosomal protein expression

miR-132 deficiency resulted in upregulation of several RP genes in CD4⁺ T cells from chronically infected mice with *L. donovani* (**Fig. 1**). In addition, we found that miR-132-3p or miR-212-3p over-expression in mouse embryonic fibroblasts (MEFs) resulted in widespread down-regulation of RP gene mRNA levels (**Fig. 3A and EV3A**). These effects were confirmed at the protein level using Rpl27 and Rps10 as two representative RPs (**Fig. EV3B**). This allowed us to further probe the mechanism employed by miR-132 to regulate ribosomal protein gene levels. The majority of RP transcripts up-regulated in *miR-132*^{-/-} mice (**Fig. 1D**) lacked miR-132/212-3p sites (13/15 coding transcripts), with the remaining 2/15 (RPL7L1 and RPL18) displaying non-conserved sites. Predicted miR-132/212-3p targets are statistically significantly enriched in proteins involved in transcription (**Fig. EV3C**). Therefore, we reasoned that the effect of miR-132 on RP gene expression was caused by miR-132-mediated suppression of transcriptional regulators. For example, p300, a previously validated miR-132 target [3], is required for the activity of Sp1, YY1 and CREB, all of which have known roles in transcription of RP genes [26-28]. Of note, although miR-132 directly suppresses p300, its effects on p300 mRNA steady-state levels are minimal [3]. In parallel, BTAF1, a predominant miR-132 target in CD4⁺ T cells (**Fig. 2**) interacts with TATA-binding protein (TBP) to form B-TFIID, causing redistribution of TBP to new genomic sites [29, 30]. Over-expression of miR-

132 in MEFs resulted in suppression of p300 and BTAF1 (**Fig. 3B**). Similarly, over-expression of miR-132-3p or miR-212-3p in the EL4 T cell line also resulted in suppression of BTAF1 and p300 (**Fig. EV3D**) suggesting that both miRNAs contribute to regulation of BTAF1 and p300. Knockdown of p300 resulted in significant downregulation of several miR-132-regulated RP transcript levels, including RPL27, RPSA, RPS3A, RPS9, RPS10, and RPL14-ps1 (**Fig. 3C**), whereas levels of RPL18 showed a trend towards downregulation ($P=0.06$). In addition, knockdown of BTAF1 significantly reduced levels of RPL27 and RPL18, with RPL14-ps1 showing a trend towards downregulation ($P=0.052$) (**Fig. 3D**). Critically, suppression of RP expression by miR-132 was dependent on both p300 and BTAF1 (**Fig. 3E**). Although the majority of miR-132-mediated effects on RP expression were abolished upon knockdown of either p300 or BTAF1, we also identified RP mRNAs that were specifically dependent on p300 (e.g. miR-132-mediated suppression of Rps9) or BTAF1 (e.g. miR-132-mediated suppression of Rpl18; **Fig. 3E**). To validate the functional relevance of these effects we tested protein synthesis rates in MEFs over-expressing miR-132-3p or miR-212-3p using a puromycin incorporation assay [31]. Over-expression of either of the two miRNAs resulted in suppression of protein synthesis, consistent with their effect on RP expression (**Fig. 3F**). These findings demonstrate that p300 and BTAF1, two miR-132 targets involved in transcription, contribute towards the widespread regulation of RP genes observed in miR-132/212-deficient or over-expressing cells. Interestingly, Mot1, the yeast homologue of BTAF1, promotes expression of ribosomal proteins in yeast [32], as seen here for BTAF1 and RPL27 and RPL18 in mouse cells. We should note that given the number of potential miR-132 targets involved in transcription (**Fig. EV3C**) [33], we cannot exclude the contribution of additional miR-132 targets towards RP gene regulation. Importantly, it is thought that the majority of RP genes are not regulated at the post-transcriptional level by miRNAs due their relatively short 3'UTRs [34]. However, our work demonstrates that a miRNA can indirectly suppress a cluster of RP genes in CD4⁺ T cells and MEFs. This reveals a novel mechanism of RP regulation with miR-132

acting as a molecular node mediating crosstalk between RP expression and post-transcriptional gene silencing.

The miR-212/132 cluster controls the balance between IL-10 and IFN γ production in CD4⁺ T cells.

Having shown that miR-132 deficiency results in similar transcriptomic effects in CD4⁺ cells *in vitro* and *in vivo* (e.g. RP gene regulation, BTA1 suppression) and during *L. donovani* infection (**Figs. 1 and 2**), we measured capacity for IFN γ and IL-10 production by CD4⁺ T cells from infected mice by intracellular cytokine staining following *ex vivo* stimulation with PMA and ionomycin. We found a modest but significant reduction in the ability of *miR-132*^{-/-} CD4⁺ T cells to produce IFN γ (**Fig. 4A**). This was accompanied by a greater fold increase in production of IL-10 by *miR-132*^{-/-} IFN γ ⁺ CD4⁺ T cells compared to wild-type cells (**Fig. 4B and Fig. EV4A**). Interestingly, IL-10 mRNA levels were not statistically significantly different between *WT* and *miR-132*^{-/-} cells (**Fig. 4C**), indicating that miR-132 affected IL-10 expression at the post-transcriptional/translational level. Increased IL-10 production by *miR-132*^{-/-} CD4⁺ T cells was also evident following *in vitro* restimulation of splenic CD4⁺ T cells from infected mice with *L. donovani* antigen demonstrating that the effect was occurring in antigen-specific manner (**Fig. EV4B**). The observed reduction in frequency of IFN γ ⁺ CD4⁺ T cells and an increase in frequency of IFN γ ⁺IL-10⁺ CD4⁺ T cells is consistent with the concept that IL-10⁺ Th1 cells develop after prolonged exposure to antigen and represent an endpoint of the Th1 response [35]. In this respect, our results can be interpreted as *miR-132*^{-/-} CD4⁺ T cells reaching this endpoint immunoregulatory status prematurely.

At the molecular level, the increase in IFN γ ⁺IL-10⁺ CD4⁺ T cells *in vivo* was associated with a transcriptomic signature characterised by an up-regulation of a cluster of RP genes in *miR-132*^{-/-} CD4⁺ T cells (**Fig. 1D-E**). To further explore this finding we compared *in vitro* Th1 differentiation of *WT* and *miR-132*^{-/-} CD4⁺ T cells in presence or absence of phenylephrine (PE), which has been shown to enhance ribosome biosynthesis [36].

277 Remarkably, although there were no statistically significant differences between *miR*-
278 *132*^{-/-} and WT cells, nor between WT DMSO-treated and PE-treated cells, treating *miR*-
279 *132*^{-/-} CD4⁺ T cells with PE resulted in statistically significantly enhanced IL-10
280 expression and increased number of cells compared to WT cells. An increase in IL-10
281 levels was observed in PE-treated WT cells compared to DMSO-treated WT cells but
282 this did not reach statistical significance. IFN γ levels were not affected by PE and were
283 lower in *miR*-*132*^{-/-} Th1 cells although this did not reach significance after multiple testing
284 correction (**Fig. 4D-F**). In agreement with our *in vivo* observations, the enhanced cell
285 number and IL-10 expression under these *in vitro* conditions recapitulated enhanced
286 activation and premature acquisition of an immunoregulatory state in *miR*132^{-/-} CD4⁺ T
287 cells. Overall, these results demonstrated that miR-132 connects RP expression, IL-10
288 expression, and CD4⁺ T cell activation in Th1 cells. Our results infer that the observed
289 deregulation of selected RPs in *miR*-*132*^{-/-} CD4⁺ T cells *in vivo* likely alters the
290 composition and function of ribosomes in a manner that specifically promotes IL-10
291 expression. This could be potentially explained by formation of specialised ribosomes in
292 activated CD4⁺ T cells [37, 38].

293

294 **The miR-212/132 cluster promotes protective immunity to *L. donovani*.**

295 Having observed that loss of miR-132 favours an immunoregulatory (higher IL-10
296 expression) phenotype in Th1 cells, we tested the response of miR-132^{-/-} mice to *L.*
297 *donovani* infection. Indeed, IFN γ ⁺IL-10⁺ CD4⁺ T cells have been associated with immune
298 dysregulation and infection susceptibility in a variety of human and experimental
299 systems [39-43]. Furthermore, the role of IL-10 in preventing *L. donovani* clearance had
300 been previously demonstrated [44-46]. However this support comes from the study of
301 fully IL-10-deficient mice and use of blocking antibodies against IL-10 or its receptor. To
302 determine whether modest changes in IL-10 levels could alter infection outcomes, we
303 infected *IL*-10^{+/+}, *IL*-10^{+/-} and *IL*-10^{-/-} mice. Infected *IL*-10^{+/-} mice produced intermediate
304 levels of IL-10 compared to their *IL*-10^{+/+} and *IL*-10^{-/-} counterparts (**Fig. EV5A**), without

305 any change in IFN γ production (**Fig. EV5B**). Notably, as with WT mice treated with IL-
 306 10R-blocking antibody or *IL-10*^{-/-} mice, *IL-10*^{+/-} mice were able to clear liver parasites
 307 albeit with slower kinetics (**Fig. 5A**). These experiments suggested that modifying the
 308 relative abundance of IL-10 and IFN γ by reducing IL-10 by 50% can affect susceptibility
 309 to *L. donovani* infection. Consistently with these findings and the observed IL-10 levels
 310 in *miR-132*^{-/-} mice, *L. donovani* infection resulted in significantly elevated splenic
 311 parasite burdens in *miR-132*^{-/-} mice (**Fig. 5B**). Although we observed variation in parasite
 312 load between different experiments (**Fig. 5C**), *miR-132*^{-/-} spleens consistently harboured
 313 approximately 2-fold more parasites at day 28 compared to WT controls (**Fig. 5C-D**). In
 314 addition to parasite loads *miR-132* deficiency affected CD11b⁺ cell populations, here
 315 called M ϕ A (CD11b⁺ F4/80⁺ CD11c⁻), M ϕ B (CD11b^{hi} F4/80^{hi} CD11c⁺), and M ϕ C
 316 (CD11b^{hi} F4/80^{lo} CD11c⁺) present in infected spleens (gated as **Fig. EV5C**). The
 317 numbers of M ϕ A and M ϕ B cells decreased in infected *miR-132*^{-/-} mice characterised by
 318 higher IL-10 expression in CD4⁺ T cells (**Fig. EV5D**). Conversely, numbers of these
 319 populations increased in an IL-10 dose dependent manner, in infected *IL-10*^{-/-} and to a
 320 lesser extent in *IL-10*^{+/-} mice (**Fig. EV5E**), demonstrating that the number of these cells
 321 is inversely correlated with IL-10 expression. Of note, IL-10 expression did not differ
 322 between *WT* and *miR-132*^{-/-} myeloid subpopulations (**Fig. EV5F**). This demonstrated
 323 that the effect of *miR-132* on IL-10 expression does not occur in all IL-10-producing cell
 324 types, showing specificity for Th1 cells. Our findings do not exclude that *miR-132*-
 325 mediated suppression of IL-10 might occur in other cell types (e.g. B cells, innate
 326 lymphoid cells) contributing to the overall function of *miR-132* in immunity.
 327 Liver parasite burdens peaked around day 21 and we noted increased levels in *miR*-
 328 132^{-/-} mice at this time point (**Fig. EV5G**). Whilst *miR-132*^{-/-} liver burdens were only
 329 significantly elevated at day 28 when we corrected for inter-experiment variations in
 330 infection intensity (**Fig. EV5H**), *miR-132*^{-/-} mice continued to harbour a significantly
 331 elevated parasite burden at day 42 (**Fig. EV5I**), a time point when parasites are being
 332 cleared from this organ in WT C57BL/6 mice [18]. Notably, the enhanced pathogen

burdens coincided with significantly smaller spleen and liver size in *miR-132*^{-/-} mice compared to their WT counterparts (**Fig. 5E-F**). The impact of miR-132 deficiency on hepatosplenomegaly was most pronounced at higher infection levels, with a similar trend also evident after infection with lower parasite doses (**Fig. EV5J-K**).

In sum, we propose that our findings support a model according to which enhanced ribosomal protein expression upon activation of *miR-132*^{-/-} CD4⁺ T cells *in vivo* contributes towards accelerated activation of these cells and the premature switch to the IFN γ ⁺IL-10⁺ phenotype. Although we cannot exclude that other cell types or mechanisms contribute to the observed increase in parasite loads in *miR-132*^{-/-} mice, we propose that the effects of miR-132 deficiency on IL-10 expression in IFN γ ⁺ CD4⁺ T cells significantly contribute to reduced protective inflammation and enhanced susceptibility of *miR-132*^{-/-} mice to infection. This is consistent with previous publications that highlight that IL-10 produced by Th1 cells (rather than regulatory T cells or myeloid cells) is a critical determinant of *L. donovani* infection outcomes [40, 47]. Of note, due to the impossibility of concurrent physiological knockdown or over-expression of RPs, the functional relevance of this family of proteins to Th1 responses *in vivo* has remained elusive. Our results provide a novel conceptual framework for the *in vivo* relevance of RP expression in CD4⁺ T cells indicating that exaggerated RP expression can be associated with impaired T cell responses. We propose that miR-132-driven coordination of the machineries that control RNA metabolism is essential for optimal Th1 cell activation and protective immunity.

MATERIALS AND METHODS

Ethics

Animal care and experimental procedures were regulated under the Animals (Scientific Procedures) Act 1986 (revised under European Directive 2010/63/EU) and were performed under UK Home Office License (project licence number PPL 60/4377 with approval from the University of York Animal Welfare and Ethical Review Body). Animal

361 experiments conformed to ARRIVE guidelines.

362

363 **Mice and *L. donovani* infection**

364 Female C57BL/6 CD45.1, CD45.2, and RAG2^{-/-} mice were obtained from Charles River
365 (UK). *MiR-132/212*^{-/-} mice (complete knockouts) were provided by Dr Richard Goodman
366 (Vollum Institute, Oregon Health & Science University, USA). IL-10^{-/-} mice were provided
367 by Dr Anne O'Garra (Francis Crick Institute, UK) and were crossed with WT CD45.2
368 C57BL/6 mice to generate IL-10^{+/-} heterozygotes. All mice were bred in house,
369 maintained under specific pathogen-free conditions and used at 6 – 12 weeks of age.
370 The Ethiopian strain of *L. donovani* (LV9) was maintained by passage in RAG-2^{-/-} mice.
371 Mice were infected i.v. with 100x10⁶ amastigotes via the tail vein. Parasite doses of 10
372 and 30x10⁶ were also used where indicated. Parasite burden was expressed as
373 Leishman-Donovan units (LDU; the number of parasites per 1,000 host cell nuclei ×
374 organ weight in mg)[48]. To allow comparison between these experiments, we
375 normalised LDU to the levels observed in WT mice (relative LDU). For IL-10R
376 neutralisation experiments mice were infected with *L. donovani* and received anti-IL10R
377 (Clone: 1B1.3A from Bio X Cell) or IgG isotype control (SIGMA) injections at day 0, 14,
378 and 21 p.i. at 0.5mg mAb/injection.

379

380 **FACS analysis and cell sorting.**

381 For FACS analysis, spleens were first digested with 0.4 U/ml Liberase TL (Roche) and
382 80 U/ml DNase I type IV in Hank's Balanced Salt Solution (both Sigma) for 15min at
383 37°C. Enzyme activity was inhibited with 10mM EDTA pH 7.5 and single cell
384 suspensions created with 70 µm nylon filters (BD Biosciences) in complete RPMI 1640
385 (ThermoFisher) supplemented with 10% heat inactivated FCS (HyClone), 100 U/ml
386 penicillin, 100 µg/ml streptomycin and 2 mM L-glutamine (all ThermoFisher). Red blood
387 cells were lysed with red blood cell lysing buffer (Sigma), For live/dead discrimination,
388 cells were washed twice in PBS, then stained with Zombie Aqua (Biolegend) before

389 resuspension in FACS buffer (PBS containing 0.5% BSA and 0.05% azide). Fc
390 receptors were blocked with 100µg/ml rat IgG (Sigma) for 10min at 4°C, before surface
391 staining for 30min at 4°C. Combinations of the following anti-mouse antibodies were
392 used: CD45.1 APC (clone A20); CD45.2 BV786 (104); CD3 FITC (145-2C11); B220
393 FITC (RA3-6B2); TCRβ PE-Cy7 (H57-597); MHCII alexa700 (M5/114.15.2); Ly6G PE-
394 Cy7 (1A8); CD11b PB and APC (M1/70); CD11c PerCP/Cy5.5 (N418); F4/80 FITC and
395 alexa647 (BM8); CD44 FITC (IM7); CD62L PE (MEL-14); CD8α APC (53-6.7); CD4 PE
396 and PerCP/Cy5.5 (RM4-5); IFNγ FITC (XMG1.2); IL-10 PE (JES5-16E3). All antibodies
397 were from Biolegend. To measure intracellular cytokines in T cells following *ex vivo*
398 stimulation, cells were first stimulated in complete RPMI for 4 hours at 37°C with
399 500ng/ml PMA, 1µg/ml ionomycin and 10µg/ml brefeldin A (all Sigma). For myeloid cells,
400 cells were cultured as above either in the absence of exogenous stimulation (brefeldin
401 A alone) or with *E. coli* O55:B5 LPS (1µg/ml with brefeldin A; Sigma). To measure
402 antigen-specific cytokine production, CD4⁺ cells were purified by magnetic separation
403 (Miltenyi Biotec) from the spleens of day 28 *L. donovani* infected CD45.2 WT and miR-
404 132^{-/-} mice and cultured for 3 days with naïve splenocytes (CD45.1 WT mice) as a source
405 of antigen-presenting cells (0.5x10⁶ CD45.2⁺ *Ld* CD4⁺, 1x10⁶ CD45.1⁺ naïve
406 splenocytes). Cells were cultured either alone or with 1.5x10⁷ whole killed (freeze-
407 thawed) *L. donovani* amastigotes as a source of parasite antigen. Brefeldin A was added
408 as above for the final 4 hours of culture to permit accumulation of intracellular cytokines.
409 CD45.2 and CD45.1 staining was used to assess cytokine production by CD4 T cells
410 from *L. donovani*-infected and naïve mice, respectively. For all intracellular cytokine
411 staining, surface stained cells were fixed and permeabilised (20min at 4°C) using
412 Fixation/Permeabilisation solution before washes in Perm/Wash buffer (both BD
413 Biosciences). Cells were then staining with intracellular antibodies as above except in
414 Perm/Wash buffer. Appropriate isotype controls were included. For FACS analysis,
415 events were acquired on a LSRFortessa (BD Biosciences) before analysis with FlowJo
416 (FlowJo LLC). For cell sorting of splenic lymphocytes from naïve and *Ld*-infected

417 spleens, B cells were gated as B220⁺ CD3⁻; CD4 T cells as B220⁻ CD3⁺ CD4⁺ CD8a⁻;
418 and CD8 T cells as B220⁻ CD3⁺ CD4⁻ CD8a⁺. For purification of naïve and activated CD4
419 T cells from uninfected mice, single cell suspensions were prepared from pooled
420 spleens and peripheral LN (axillary, brachial and inguinal). CD4⁺ cells were enriched
421 using CD4 microbeads and LS columns (both Miltenyi Biotec) before cell sorting of naïve
422 CD4 T cells (CD4⁺ CD62L⁺ CD44⁻ CD11b⁻ CD8a⁻ MHCII⁻). For cell sorting of splenic
423 myeloid cell populations, cells were gated as Fig. EV5C. Cell sorting was performed with
424 a MoFlo Astrios (Beckman Coulter) and sorted cells were typically >98% positive.

425

426 ***In vitro* activation of CD4 T cells**

427 Purified CD4 T cells were stimulated with 10µg/ml plate bound anti-CD3ε (clone 145-
428 2C11) and 2µg/ml soluble anti-CD28 (37.51) in RPMI 1640 as before in flat bottom 96
429 well plates. For Th1 polarisation, cells were also treated with 15ng/ml recombinant
430 mouse IL-12 and 5µg/ml anti-IL-4 (11B11), or for Th2 polarisation, 30ng/ml recombinant
431 mouse IL-4 and 5µg/ml anti-IFNγ (XMG1.2). Phenylephrine hydrochloride (Sigma) was
432 used at 10µM and added during both anti-CD3 dependent activation (4 days) and also
433 during rest in 10U/ml recombinant human IL-2 (2 days). All antibodies were from
434 Biolegend and were low endotoxin / azide free, and recombinant cytokines were from
435 Peprotech.

436

437 **MEF cell culture, siRNA and miRNA mimic treatment**

438 C57BL/6 MEFs were provided by Dr. D. Coverley (University of York, UK) and were
439 cultured in DMEM (high glucose and pyruvate; ThermoFisher) supplemented with 10%
440 FCS, pen-strep and L-glut as RPMI. For transfections, 5x10⁴ cells per well were seeded
441 in 6 well plates and transfected the next day with ON-TARGETplus SMARTpool siRNA
442 (100nM), miRIDIAN miRNA mimics (50nM), or appropriate controls (all Dharmacon, GE
443 Healthcare) using TransIT-siQUEST transfection reagent (Mirus) and Opti-MEM
444 medium (ThermoFisher) for 6 hours before being replaced with complete DMEM. EL4

445 cells were grown in RPMI supplemented with 10% FCS and were transfected with
446 miRNA mimics using Neon Nucleofection as per manufacturer's instructions. Non-
447 targeting control (NTC) siRNAs or mimics were used as controls. Cells were harvested
448 48 hours after transfection.

449

450 **Quantitative reverse transcription PCR (qRT-PCR)**

451 RNA was extracted from tissue samples or purified cell populations using QIAzol and
452 miRNeasy RNA extraction kits (QIAGEN) according to manufacturer's instructions.
453 Tissue samples were first dissociated in QIAzol using a TissueLyser LT with stainless
454 steel beads (all QIAGEN, UK). For detection of mature miRNA, cDNA was synthesised
455 using Taqman miRNA reverse transcription kits, and levels determined with Taqman
456 miRNA assays and Taqman Universal PCR Master Mix (all ThermoFisher). For mRNA
457 transcripts, reverse transcriptions were carried out with Superscript III (ThermoFisher)
458 and random hexamer primers (Promega), and measured with Fast SYBR Green Master
459 Mix (ThermoFisher). PCR were performed using a StepOnePlus Real Time PCR
460 System (ThermoFisher) and relative transcript levels determined using the $\Delta\Delta C_t$ method.
461 Mature miRNA levels were normalised to U6. RNA transcript levels in T cells from *L.*
462 *donovani*-infected mice and MEFs were normalised to HPRT. As *in vitro* CD4 T cell
463 activation changes HPRT, GAPDH and β -actin expression levels, U6 was also used to
464 normalise mRNA expression in day 0 and 1 naïve T cells. The following primer
465 sequences were used:

466 BTAF1: Forward: 5'GCCTTTGGAAAGCTTTTGTG3', Reverse:

467 5'CCAGTACCTGCCCCATGT3'. HPRT: Forward:

468 5'GCGTCGTGATTAGCGATGATGAAC3', Reverse:

469 5'ATCTCCTTCATGACATCTCGAGCAAGTC3'. POLR2F: Forward:

470 5'GAGGAGGACGAAGGACTTGA3', Reverse: 5'CCAGATGGGAGAATCTCGAC3'.

471 RPL12: Forward: 5'CGAAGATCGGTCCTCTGG3', Reverse:

472 5'AATTCTGAGACCCTTCCAGTCA3'. RPL18: Forward:

473 5'CGCATGATCCGAAAGATGA3', Reverse: 5'AACTTCCAGAATCCGCACAT3'.
 474 RPL26: Forward: 5'AGAAGGCTAATGGCACAACC3', Reverse:
 475 5'TCCAGCTTTAGCCTGGTGAT3'. RPL27: Forward:
 476 5'TGAAAGGTTAGCGGAAGTGC3', Reverse: 5'CATGAACTTGCCCATCTCG3'.
 477 RPL8: Forward: 5'CAACAGAGCCGTTGTTGGT3', Reverse:
 478 5'CAGCCTTTAAGATAGGCTTGTCAT3'. RPS10: Forward:
 479 5'GTGAGCGACCTGCAAGATTC3', Reverse: 5'CAGCCTCAGCTTTCTTGTCAT3'.
 480 RPS14: Forward: 5'AGTCTGGAGACGACGATCAGA3', Reverse:
 481 5'CAGACACCAAACACATTCTCTCC3'. RPS30: Forward:
 482 5'GGTCGCCCAGATCAAAGAT3', Reverse: 5'TGCCAGAAGCACGACTTG3'. RPS3A:
 483 Forward: 5'TGGCAAGAAGGGAGCTAAGA3', Reverse:
 484 5'GTGTCTTCCCGATGTTCTTAAT3'. RPS9: Forward:
 485 5'ATCCGCCAACGTCACATTA3', Reverse: 5'TCTTCACTCGGCCTGGAC3'. RPSA:
 486 Forward: 5'GGTCCATACGGCGTTGTT3', Reverse:
 487 5'GCAGCAAGGAATTTGAGGAC3'. RPL14-ps1: Forward:
 488 5'TGCTGCTGCTGCTAAAGCTA3', Reverse: 5'CAGCCTTCTTGCTGGTC3'. RPL23-
 489 ps3: Forward: 5'ATAAGGCCCGACGGAGAG3', Reverse:
 490 5'GAATTAGCCATCTGGACTCAGTTT3'.

491

492 **SDS-PAGE, Western blotting, and protein synthesis assays**

493 Cells were washed twice in PBS and protein extracts prepared in RIPA buffer (150mM
 494 NaCl, 10mM Tris pH 7.2, 5mM EDTA, 0.1% SDS, 0.1% Triton X-100, 1% sodium
 495 deoxycholate, 1mM PMSF, 1% Protease Inhibitor cocktail P8340, 1% Phosphate
 496 Inhibitors cocktails 2 and 3; all Sigma). Equal total amounts of protein were resolved on
 497 SDS-PAGE gels and transferred to PVDF membranes (Millipore) using a BioRad SD
 498 Semidry Transfer Cell, blocked for 2 hours at room temperature in 2% BSA
 499 (ThermoFisher) or 5% milk powder (Sigma) in TBST (150mM NaCl, 7.7mM Tris HCl pH
 500 8, 0.1% Tween 20; all Sigma) before overnight probing with primary antibodies at 4°C.

501 Antibodies were as follows: total CREB (clone 48H2), p-CREB S133 (87G3), BTA1
502 (rabbit pAb #2637; all Cell Signaling Technology), p300 (clone NM11), Rpl27 (14980-1-
503 AP, Proteintech), Rps9 (14894-1- AP, Proteintech), β -actin (AC-15), GAPDH (9484; all
504 Abcam). Following extensive washing in TBST, blots were incubated with secondary
505 antibodies (goat anti-rabbit or mouse HRP; DAKO) for 1 hour at room temp, washed as
506 before, and developed with ECL Western Blotting Detection Reagent and Hyperfilm ECL
507 (both GE Healthcare). Densitometry was performed using Fiji / ImageJ.

508 Protein synthesis rates were measured by puromycin incorporation [31]. Cells were
509 pulsed for 10 mins with 10 μ g/ml puromycin (Sigma) and then washed and incubated for
510 an extra 50 mins before lysed and used for western blotting analysis. Puromycin was
511 detected with the monoclonal antibody clone 12D10 (Merck Millipore).

512

513 **RNA sequencing analysis**

514 Sequence reads were trimmed to remove adaptor sequences with Cutadapt and
515 mapped to mouse genome GRCm38 with HISAT2[49] including “rna-strandness FR”
516 option. Data available at GEO, accession number GSE125268. Transcriptome
517 assembly and quantification was performed using the Tuxedo pipeline (version
518 2.2.1)[50]. Cufflinks was used to assemble transcriptomes for each sample using the
519 GTF annotation file for the GRCm38 mouse genome. This was followed by running
520 Cuffmerge to merge individual sample transcriptomes into full transcriptomes.
521 Quantification and normalisation were carried out for each experiment using Cuffquant
522 and Cuffnorm. Differential expression on gene FPKM values was performed by
523 conducting paired and independent t-tests with Benjamini-Hochberg false discovery rate
524 correction. GSEA (<http://software.broadinstitute.org/gsea>) and STRING analysis
525 (<http://string-db.org/>) were performed where indicated. For analysis of genes
526 differentially expressed between WT and miR-132^{-/-} CD4 T cells from *Ld*-infected
527 spleens, transcripts were required to be significantly dysregulated (>50% change from
528 WT levels, $p < 0.05$) with FPKM values >1, and STRING settings were highest confidence

529 interactions only excluding text mining. Targetscan (http://www.targetscan.org/vert_71/)
530 was used to predict targets of miRNA from the miR-212/132 cluster (cumulative
531 weighted context score++ <-0.1).

532

533 **Luciferase assays**

534 BTAF1 3'UTR was amplified from mouse spleen cDNA (reverse transcribed with
535 Superscript II and oligo-dT primers; both ThermoFisher) using the following primers :
536 forward 5'CTCGAGTGCAACTGCTGCTAGCTCAGTTA3' (which introduces 5' Xho I
537 site) and reverse 5'GCGGCCGCTTATGAAAGCAGACAAGTA3' (which introduces 3'
538 Not I site). The 1.5 kb amplicon, which encompasses most of the 3' UTR of BTAF1
539 minus a 25nt 5' GC rich stretch, was cloned into pGEM-T vector (Promega) and
540 sequence verified. We also performed site directed mutagenesis to remove the miR-
541 212/132 seed sequence using QuikChange Site-Directed Mutagenesis (Agilent) with the
542 following primer pairs :

543 5'CTGAACCCTGTGGTAAAGACT**AA**ATACTGTAGCAGGGCCTGAAGC3' and
544 5'GCTTCAGGCCCTGCTACAGTATTTAGTCTTTACCACAGGGTTCAG3', resulting in
545 mutation of WT sequence (5'AACCCUGUGGUAAGACUG**UUU**U3') to mutant
546 (5'AACCCUGUGGUAAGACU**AAU**U3'). Inserts were excised with XhoI and NotI
547 (NEB) and ligated into psiCHECK-2 (Promega). Luciferase assays were performed in
548 HeLa and 3T3 cells 24 hours after transfection as previously described[3].

549

550 **Statistical analysis**

551 Statistical analyses were carried out as indicated with Prism 5 (Graphpad Software Inc).
552 Two-way comparisons used paired or unpaired t-tests as indicated and multiple
553 comparisons used one-way ANOVA, followed by Bonferroni correction for multiple
554 testing. P values of <0.05 were considered significant. * p<0.05, ** p<0.01, *** p<0.001,
555 **** p<0.0001. Statistical significance in enrichment of RP genes (as in Fig. 2I) were
556 determined using Chi-Square test.

557

558 **ACKNOWLEDGEMENTS**

559 The study was funded by the UK Medical Research Council through a New Investigator
560 Research Grant (MR/L008505/1) awarded to D.L., a Programme Grant awarded to
561 P.M.K. (G1000230), and a project Grant awarded to T.V.S. (MR/N009185/1). We would
562 like to thank Dr R. Goodman and Dr G. Zhang for providing the *miR-132/miR-212*
563 knockout mice, Dr A. O'Garra for the *IL-10* knockout mice, and Dr M. Kullberg for helpful
564 discussions. We thank staff at the Imaging and Cytometry Lab in the University of York
565 Bioscience Technology Facility for cell sorting and imaging support and advice.

566

567 **AUTHORS CONTRIBUTIONS**

568 D.L. conceived, designed, and supervised the project. D.L. and J.P.H. designed
569 experiments. P.M.K. and T.V.S. contributed to experimental design. J.P.H., K.M.S., N.B.,
570 P.G., S.A.H. and D.L. performed experiments. J.P.H., K.N., K.M.S., and D.L. analysed
571 experiments. J.P.H. and D.L. wrote the manuscript. All authors critiqued and edited the
572 manuscript.

573

574 **CONFLICT OF INTERESTS**

575 The authors declare no conflict of interest.

576

577 **REFERENCES**

- 578 1. Mehta A, Baltimore D (2016) MicroRNAs as regulatory elements in immune
579 system logic. *Nat Rev Immunol* **16**: 279-94
- 580 2. Wanet A, Tacheny A, Arnould T, Renard P (2012) miR-212/132 expression
581 and functions: within and beyond the neuronal compartment. *Nucleic Acids Res*
582 **40**: 4742-53

- 583 3. Lagos D, Pollara G, Henderson S, Gratrix F, Fabani M, Milne RS, Gotch F,
584 Boshoff C (2010) miR-132 regulates antiviral innate immunity through
585 suppression of the p300 transcriptional co-activator. *Nat Cell Biol* **12**: 513-9
- 586 4. Nahid MA, Yao B, Dominguez-Gutierrez PR, Kesavalu L, Satoh M, Chan
587 EK (2013) Regulation of TLR2-mediated tolerance and cross-tolerance through
588 IRAK4 modulation by miR-132 and miR-212. *J Immunol* **190**: 1250-63
- 589 5. Shaked I, Meerson A, Wolf Y, Avni R, Greenberg D, Gilboa-Geffen A, Soreq
590 H (2009) MicroRNA-132 potentiates cholinergic anti-inflammatory signaling by
591 targeting acetylcholinesterase. *Immunity* **31**: 965-73
- 592 6. Taganov KD, Boldin MP, Chang KJ, Baltimore D (2006) NF-kappaB-
593 dependent induction of microRNA miR-146, an inhibitor targeted to signaling
594 proteins of innate immune responses. *Proc Natl Acad Sci U S A* **103**: 12481-6
- 595 7. Mehta A, Mann M, Zhao JL, Marinov GK, Majumdar D, Garcia-Flores Y, Du
596 X, Erikci E, Chowdhury K, Baltimore D (2015) The microRNA-212/132 cluster
597 regulates B cell development by targeting Sox4. *J Exp Med* **212**: 1679-92
- 598 8. Mehta A, Zhao JL, Sinha N, Marinov GK, Mann M, Kowalczyk MS, Galimidi
599 RP, Du X, Erikci E, Regev A, *et al.* (2015) The MicroRNA-132 and MicroRNA-
600 212 Cluster Regulates Hematopoietic Stem Cell Maintenance and Survival with
601 Age by Buffering FOXO3 Expression. *Immunity* **42**: 1021-32
- 602 9. Hanieh H, Alzahrani A (2013) MicroRNA-132 suppresses autoimmune
603 encephalomyelitis by inducing cholinergic anti-inflammation: a new Ahr-based
604 exploration. *Eur J Immunol* **43**: 2771-82
- 605 10. Iliopoulos D, Jaeger SA, Hirsch HA, Bulyk ML, Struhl K (2010) STAT3
606 activation of miR-21 and miR-181b-1 via PTEN and CYLD are part of the
607 epigenetic switch linking inflammation to cancer. *Mol Cell* **39**: 493-506

- 608 11. Li D, Wang A, Liu X, Meisgen F, Grunler J, Botusan IR, Narayanan S, Erikci
609 E, Li X, Blomqvist L, *et al.* (2015) MicroRNA-132 enhances transition from
610 inflammation to proliferation during wound healing. *J Clin Invest* **125**: 3008-26
- 611 12. Xiao J, Li Y, Prandovszky E, Karuppagounder SS, Talbot CC, Jr., Dawson
612 VL, Dawson TM, Yolken RH (2014) MicroRNA-132 dysregulation in *Toxoplasma*
613 *gondii* infection has implications for dopamine signaling pathway. *Neuroscience*
614 **268**: 128-38
- 615 13. Ni B, Rajaram MV, Lafuse WP, Landes MB, Schlesinger LS (2014)
616 *Mycobacterium tuberculosis* decreases human macrophage IFN-gamma
617 responsiveness through miR-132 and miR-26a. *J Immunol* **193**: 4537-47
- 618 14. Magill ST, Cambronne XA, Luikart BW, Liou DT, Leighton BH, Westbrook
619 GL, Mandel G, Goodman RH (2010) microRNA-132 regulates dendritic growth
620 and arborization of newborn neurons in the adult hippocampus. *Proc Natl Acad*
621 *Sci U S A* **107**: 20382-7
- 622 15. Asmal M, Colgan J, Naef F, Yu B, Lee Y, Magnasco M, Luban J (2003)
623 Production of ribosome components in effector CD4⁺ T cells is accelerated by
624 TCR stimulation and coordinated by ERK-MAPK. *Immunity* **19**: 535-48
- 625 16. Vo N, Klein ME, Varlamova O, Keller DM, Yamamoto T, Goodman RH,
626 Impey S (2005) A cAMP-response element binding protein-induced microRNA
627 regulates neuronal morphogenesis. *Proc Natl Acad Sci U S A* **102**: 16426-31
- 628 17. Kaiser M, Wiggin GR, Lightfoot K, Arthur JS, Macdonald A (2007) MSK
629 regulate TCR-induced CREB phosphorylation but not immediate early gene
630 transcription. *Eur J Immunol* **37**: 2583-95
- 631 18. Kaye P, Scott P (2011) Leishmaniasis: complexity at the host-pathogen
632 interface. *Nat Rev Microbiol* **9**: 604-15

- 633 19. Rodriguez A, Vigorito E, Clare S, Warren MV, Couttet P, Soond DR, van
634 Dongen S, Grocock RJ, Das PP, Miska EA, *et al.* (2007) Requirement of
635 bic/microRNA-155 for normal immune function. *Science* **316**: 608-11
- 636 20. Yang L, Boldin MP, Yu Y, Liu CS, Ea CK, Ramakrishnan P, Taganov KD,
637 Zhao JL, Baltimore D (2012) miR-146a controls the resolution of T cell responses
638 in mice. *J Exp Med* **209**: 1655-70
- 639 21. Grigoryev YA, Kurian SM, Hart T, Nakorchevsky AA, Chen C, Campbell D,
640 Head SR, Yates JR, 3rd, Salomon DR (2011) MicroRNA regulation of molecular
641 networks mapped by global microRNA, mRNA, and protein expression in
642 activated T lymphocytes. *J Immunol* **187**: 2233-43
- 643 22. Subramanian A, Tamayo P, Mootha VK, Mukherjee S, Ebert BL, Gillette
644 MA, Paulovich A, Pomeroy SL, Golub TR, Lander ES, *et al.* (2005) Gene set
645 enrichment analysis: a knowledge-based approach for interpreting genome-wide
646 expression profiles. *Proc Natl Acad Sci U S A* **102**: 15545-50
- 647 23. Szklarczyk D, Franceschini A, Wyder S, Forslund K, Heller D, Huerta-
648 Cepas J, Simonovic M, Roth A, Santos A, Tsafou KP, *et al.* (2015) STRING v10:
649 protein-protein interaction networks, integrated over the tree of life. *Nucleic Acids*
650 *Res* **43**: D447-52
- 651 24. Stubbington MJ, Mahata B, Svensson V, Deonaraine A, Nissen JK, Betz AG,
652 Teichmann SA (2015) An atlas of mouse CD4(+) T cell transcriptomes. *Biol*
653 *Direct* **10**: 14
- 654 25. Tan TCJ, Knight J, Sbarrato T, Dudek K, Willis AE, Zamoyska R (2017)
655 Suboptimal T-cell receptor signaling compromises protein translation, ribosome
656 biogenesis, and proliferation of mouse CD8 T cells. *Proc Natl Acad Sci U S A*
657 **114**: E6117-E6126

- 658 26. Nosrati N, Kapoor NR, Kumar V (2014) Combinatorial action of transcription
659 factors orchestrates cell cycle-dependent expression of the ribosomal protein
660 genes and ribosome biogenesis. *FEBS J* **281**: 2339-52
- 661 27. Perry RP (2005) The architecture of mammalian ribosomal protein
662 promoters. *BMC Evol Biol* **5**: 15
- 663 28. Thomas MJ, Seto E (1999) Unlocking the mechanisms of transcription
664 factor YY1: are chromatin modifying enzymes the key? *Gene* **236**: 197-208
- 665 29. Auble DT, Wang D, Post KW, Hahn S (1997) Molecular analysis of the
666 SNF2/SWI2 protein family member MOT1, an ATP-driven enzyme that
667 dissociates TATA-binding protein from DNA. *Mol Cell Biol* **17**: 4842-51
- 668 30. Choukrallah MA, Kobi D, Martianov I, Pijnappel WW, Mischerikow N, Ye T,
669 Heck AJ, Timmers HT, Davidson I (2012) Interconversion between active and
670 inactive TATA-binding protein transcription complexes in the mouse genome.
671 *Nucleic Acids Res* **40**: 1446-59
- 672 31. Schmidt EK, Clavarino G, Ceppi M, Pierre P (2009) SUnSET, a
673 nonradioactive method to monitor protein synthesis. *Nat Methods* **6**: 275-7
- 674 32. Venters BJ, Irvin JD, Gramlich P, Pugh BF (2011) Genome-wide
675 transcriptional dependence on conserved regions of Mot1. *Mol Cell Biol* **31**:
676 2253-61
- 677 33. Alvarez-Saavedra M, Antoun G, Yanagiya A, Oliva-Hernandez R, Cornejo-
678 Palma D, Perez-Iratxeta C, Sonenberg N, Cheng HY (2011) miRNA-132
679 orchestrates chromatin remodeling and translational control of the circadian
680 clock. *Hum Mol Genet* **20**: 731-51

681 34. Ledda M, Di Croce M, Bedini B, Wannenes F, Corvaro M, Boyl PP,
682 Caldarola S, Loreni F, Amaldi F (2005) Effect of 3'UTR length on the translational
683 regulation of 5'-terminal oligopyrimidine mRNAs. *Gene* **344**: 213-20

684 35. Cope A, Le Friec G, Cardone J, Kemper C (2011) The Th1 life cycle:
685 molecular control of IFN-gamma to IL-10 switching. *Trends Immunol* **32**: 278-86

686 36. Zhang Z, Liu R, Townsend PA, Proud CG (2013) p90(RSK)s mediate the
687 activation of ribosomal RNA synthesis by the hypertrophic agonist phenylephrine
688 in adult cardiomyocytes. *J Mol Cell Cardiol* **59**: 139-47

689 37. Segev N, Gerst JE (2018) Specialized ribosomes and specific ribosomal
690 protein paralogs control translation of mitochondrial proteins. *J Cell Biol* **217**:
691 117-126

692 38. Xue S, Barna M (2012) Specialized ribosomes: a new frontier in gene
693 regulation and organismal biology. *Nat Rev Mol Cell Biol* **13**: 355-69

694 39. Anderson CF, Oukka M, Kuchroo VJ, Sacks D (2007)
695 CD4(+)CD25(-)Foxp3(-) Th1 cells are the source of IL-10-mediated immune
696 suppression in chronic cutaneous leishmaniasis. *J Exp Med* **204**: 285-97

697 40. Jankovic D, Kullberg MC, Feng CG, Goldszmid RS, Collazo CM, Wilson M,
698 Wynn TA, Kamanaka M, Flavell RA, Sher A (2007) Conventional T-
699 bet(+)Foxp3(-) Th1 cells are the major source of host-protective regulatory IL-10
700 during intracellular protozoan infection. *J Exp Med* **204**: 273-83

701 41. Nylen S, Maurya R, Eidsmo L, Manandhar KD, Sundar S, Sacks D (2007)
702 Splenic accumulation of IL-10 mRNA in T cells distinct from CD4+CD25+ (Foxp3)
703 regulatory T cells in human visceral leishmaniasis. *J Exp Med* **204**: 805-17

704 42. Owens BM, Beattie L, Moore JW, Brown N, Mann JL, Dalton JE, Maroof A,
705 Kaye PM (2012) IL-10-producing Th1 cells and disease progression are

706 regulated by distinct CD11c(+) cell populations during visceral leishmaniasis.
707 *PLoS Pathog* **8**: e1002827

708 43. Saraiva M, Christensen JR, Veldhoen M, Murphy TL, Murphy KM, O'Garra
709 A (2009) Interleukin-10 production by Th1 cells requires interleukin-12-induced
710 STAT4 transcription factor and ERK MAP kinase activation by high antigen dose.
711 *Immunity* **31**: 209-19

712 44. Gautam S, Kumar R, Maurya R, Nylen S, Ansari N, Rai M, Sundar S, Sacks
713 D (2011) IL-10 neutralization promotes parasite clearance in splenic aspirate
714 cells from patients with visceral leishmaniasis. *J Infect Dis* **204**: 1134-7

715 45. Murphy ML, Wille U, Villegas EN, Hunter CA, Farrell JP (2001) IL-10
716 mediates susceptibility to *Leishmania donovani* infection. *Eur J Immunol* **31**:
717 2848-56

718 46. Murray HW, Moreira AL, Lu CM, DeVecchio JL, Matsushashi M, Ma X,
719 Heinzl FP (2003) Determinants of response to interleukin-10 receptor blockade
720 immunotherapy in experimental visceral leishmaniasis. *J Infect Dis* **188**: 458-64

721 47. Ranatunga D, Hedrich CM, Wang F, McVicar DW, Nowak N, Joshi T,
722 Feigenbaum L, Grant LR, Stager S, Bream JH (2009) A human IL10 BAC
723 transgene reveals tissue-specific control of IL-10 expression and alters disease
724 outcome. *Proc Natl Acad Sci U S A* **106**: 17123-8

725 48. Dalton JE, Maroof A, Owens BM, Narang P, Johnson K, Brown N,
726 Rosenquist L, Beattie L, Coles M, Kaye PM (2010) Inhibition of receptor tyrosine
727 kinases restores immunocompetence and improves immune-dependent
728 chemotherapy against experimental leishmaniasis in mice. *J Clin Invest* **120**:
729 1204-16

730 49. Kim D, Langmead B, Salzberg SL (2015) HISAT: a fast spliced aligner with
731 low memory requirements. *Nat Methods* **12**: 357-60
732 50. Trapnell C, Roberts A, Goff L, Pertea G, Kim D, Kelley DR, Pimentel H,
733 Salzberg SL, Rinn JL, Pachter L (2012) Differential gene and transcript
734 expression analysis of RNA-seq experiments with TopHat and Cufflinks. *Nat*
735 *Protoc* **7**: 562-78

736

737 **FIGURE LEGENDS**

738 **Figure 1: The miR-132/212 cluster regulates RP mRNA levels in CD4⁺ T cells from**
739 **chronically infected spleens.**

740 **A.** Expression of indicated miRNAs in sorted naïve (CD62L⁺ CD44⁻) CD4⁺ T cells and
741 following *in vitro* stimulation with anti-CD3 / anti-CD28 (1-3 days), relative to levels in
742 cells prior to stimulation. Data from 3 independent experiments each using T cells pooled
743 from 4 WT mice. Significance determined by one-way ANOVA.

744 **B.** Expression of indicated miRNAs in purified spleen lymphocytes (B cells, CD4⁺ T cells
745 and CD8⁺ T cells) from d0 naïve (white) and day 28 *L. donovani*-infected (grey) mice.
746 Expression of each miRNA normalized to levels in whole naïve spleen (dotted line). Data
747 is mean + SEM of 2 experiments with cells purified from 3-5 pooled spleens.

748 **C.** Volcano plot of RNAseq gene expression in splenic WT and *miR-132*^{-/-} CD4⁺ T cells
749 from d28 *L. donovani* infected mice. Fold change determined as log2 mean FPKM (*miR*-
750 *132*^{-/-}/WT) from 4 WT and 5 *miR-132*^{-/-} mice. Transcripts significantly different between
751 WT and *miR-132*^{-/-} (p<0.05) are shown in red. Dotted box indicates transcripts
752 significantly up-regulated in *miR-132*^{-/-} CD4⁺ T cells by more than 50%.

753 **D.** STRING network analysis of significantly up-regulated transcripts in CD4⁺ T cells
754 from spleen of d28 *L. donovani* infected *miR-132*^{-/-} mice compared to WT cells. Cluster
755 of ribosomal proteins shown in green circle, with coding RP transcripts (black) and
756 pseudogenes (red) indicated. Secondary clusters are shown in grey.

757 **E.** Top enriched molecular function Gene Ontology terms for genes significantly up-
758 regulated in CD4⁺ T cells from spleens of infected *miR-132*^{-/-} mice compared to WT mice.

759 **F.** Volcano plot of all RP genes in splenic WT and *miR-132*^{-/-} CD4⁺ T cells from d28 *L.*
760 *donovani* infected mice. RPL genes are shown as circles, RPS genes as triangles, and
761 pseudogenes as squares. Red symbols indicate significant difference between WT and
762 *miR-132*^{-/-} cells ($p < 0.05$) whereas black non-significant.

763 **G.** Expression of RP transcripts determined by qPCR from *L. donovani* infected d28 WT
764 (blue) and *miR-132*^{-/-} mice (red). N=9 for each WT and *miR-132*^{-/-} from 2 independent
765 infection experiments. Box extends from 25-75th percentile, whiskers are minimum and
766 maximum values, and horizontal lines indicate median. Significance determined by
767 unpaired t-test.

768 **H.** Fold change of all RP transcripts (grey) in Th1 cells compared to naïve CD4⁺ T cells.
769 Data taken from RNA sequencing experiments described in reference 24. Fold changes
770 in IL-10 (red) and IFN γ (blue) indicated for comparison. The statistical significance of
771 the observed up-regulation of RP transcripts in Th1 cells is determined by Chi-squared
772 test.

773 **Data information:** * $p < 0.05$, ** $p < 0.01$, *** $p < 0.001$.

774

775 **Figure 2: The B-TFIID cofactor BTAF1 is a direct miR-132 target in CD4⁺ T cells.**

776 **A.** Volcano plot (\log_2 (Fold Change) vs $-\log(P \text{ value})$) of RNA gene expression in
777 purified naïve CD62L⁺ CD44⁻ WT and *miR-132*^{-/-} CD4⁺ T cells. Fold change determined
778 as \log_2 mean FPKM (*miR-132*^{-/-}/WT) from 4 WT and 4 *miR-132*^{-/-} mice. Transcripts
779 significantly different between WT and *miR-132*^{-/-} cells ($p < 0.05$) shown in red.

780 **B.** Volcano plot of RNA gene expression in purified naïve CD62L⁺ CD44⁻ WT and *miR-*
781 *132*^{-/-} CD4⁺ T cells following 18hr *in vitro* stimulation with anti-CD3/anti-CD28 under Th1
782 conditions. Fold change determined as \log_2 mean FPKM (*miR-132*^{-/-}/WT) from 4 WT
783 and 4 *miR-132*^{-/-} mice. Transcripts significantly different between WT and *miR-132*^{-/-} cells
784 ($p < 0.05$) shown in red.

785 **C.** Volcano plot of transcripts containing a conserved miR-212/132-3p target site in
786 naïve CD4⁺ T cells from WT or *miR-132*^{-/-} mice.

787 **D.** Volcano plot of transcripts containing a conserved miR-212/132-3p target site in *in*
788 *vitro* polarised (Th1 condtions, 18h post stimulation) CD4⁺ T cells from WT or *miR-132*^{-/-}
789 ^{-/-} mice.

790 **E.** Volcano plot of transcripts containing a conserved miR-212/132-3p target site in
791 spleen CD4⁺ T cells from d28 *L. donovani* infected WT or *miR-132*^{-/-} mice.

792 **F.** BTAF1 transcript levels determined by qRTPCR in WT (blue) or *miR-132*^{-/-} (red) in
793 naïve (d0) and Th1 polarised for 18h (d1) CD4⁺ T cells, and CD4⁺ T cells from d28 *L.*
794 *donovani* infected WT or *miR-132*^{-/-} mice. N=8-9 for each WT and *miR-132*^{-/-}.

795 **G.** Expression of BTAF1 protein in d0 naïve and d1 (18hr) Th1-polarised WT and *miR-*
796 *132*^{-/-} CD4⁺ T cells, as determined by Western blot. Each lane from individual mouse,
797 and representative of two independent experiments.

798 **H.** Relative luciferase activity in HeLa transfected with plasmid containing WT *BTAF1*
799 3'UTR (white) or *BTAF1* 3'UTR on which the miR-132 binding site is mutated (grey)
800 downstream of renilla luciferase, in the presence of miR-132-3p or miR-212-3p mimics.
801 Error bars indicate SEM from eight replicate treatments.

802 Data information: Significance in (F) and (H) determined by unpaired t-test. * p<0.05, **
803 p<0.01.

804

805

806 **Figure 3: miR-132 and its targets p300 and BTAF1 control RP expression.**

807 **A.** mRNA levels of indicated RP transcripts determined by qRTPCR in MEFs transfected
808 with Non-targeting control (NTC) mimics (white) or miR-132-3p mimics (grey).

809 **B.** p300 and BTAF1 protein levels in MEF transfected with NTC mimics or miR-132-3p
810 mimics determined by Western blot. GAPDH was used as a loading control. Right panel
811 indicates mean + SEM of 4 experiments.

812 **C.** mRNA levels of indicated RP transcripts determined by qRTPCR in MEFs transfected
813 with NTC siRNA (white) or p300 siRNA (grey).

814 **D.** mRNA levels of indicated RP transcripts determined by qRTPCR in MEFs transfected
815 with NTC siRNA (white) or BTA1 siRNA (grey).

816 **E.** mRNA levels of indicated RP transcripts determined by qRTPCR in MEFs transfected
817 with NTC or miR-132-3p mimics and NTC siRNA or p300 or BTA1 siRNAs for 48h.
818 Levels are normalised to cells transfected with NTC siRNA and NTC mimic.

819 **F.** Puromycin incorporation (following 10-minute pulse and 50-minute chase)
820 determined by western blot in MEFs transfected with NTC or miR-132-3p or miR-212-
821 3p mimics.

822 Data information: Statistical significance is determined by unpaired t-test from 4-6
823 experiments. * $p < 0.05$, ** $p < 0.01$, *** $p < 0.001$, **** $p < 0.0001$.

824

825

826 **Figure 4: miR-132 controls the balance between IL-10 and IFN γ production in CD4 $^{+}$**
827 **T cells.**

828 **A.** Percentage of IFN γ^{+} live TCR β^{+} CD4 $^{+}$ cells from *L. donovani* infected WT (blue) or
829 *miR-132 $^{-/-}$* (red) mice, determined by intracellular cytokine staining. Data representative
830 of 3 independent experiments with 3-5 mice per group.

831 **B.** Percentage of IFN γ^{+} /IL-10 $^{+}$ live TCR β^{+} CD4 $^{+}$ cells from *L. donovani* infected WT (blue)
832 or *miR-132 $^{-/-}$* (red) mice, determined by intracellular cytokine staining. Data
833 representative of 3 independent experiments with 3-5 mice per group.

834 **C.** IL-10 mRNA levels, determined by RNA-sequencing, in TCR β^{+} CD4 $^{+}$ cells purified
835 from spleens of *L. donovani* infected WT (blue) or *miR-132 $^{-/-}$* (red) mice (n=5 per group).

836 **D.** Percentage of IFN γ^{+} WT (blue) or *miR-132 $^{-/-}$* (red) *in vitro* polarised Th1 cells (6 days)
837 in the presence or absence of phenylephrine (PE), determined by intracellular cytokine
838 staining.

839 **E.** Percentage of IL10⁺ WT (blue) or *miR-132*^{-/-} (red) *in vitro* polarised Th1 cells (6 days)
840 in the presence or absence of phenylephrine (PE), determined by intracellular cytokine
841 staining.

842 **F.** Total cell counts following *in vitro* Th1 polarisation (6 days) in the presence or absence
843 of phenylephrine (PE). For (D-E), cells were purified from 3 mice per group and 6
844 replicates performed.

845

846 Data information: For (A and B) statistical significance was determined by unpaired t-
847 test. For (D-F), significance was determined with 1-way ANOVA followed by
848 Bonferroni's multiple comparison test. * p<0.05, ** p<0.01, *** p<0.001. NS: not
849 significant.

850

851

852 **Figure 5: miR-132 promotes protective immunity to *L. donovani*.**

853 **A.** Liver LDU (Leishman Donovan units) at day 28 in infected WT mice treated with anti-
854 IL-10R antibody or isotype control antibody (left panel, n=5 mice per group), or at day
855 21 and day 28 from WT (blue), *IL-10*^{+/-} (open green circles) and *IL-10*^{-/-} (filled green
856 circles) mice (right panel n= 3-6 mice per group)

857 **B.** Day 28 splenic parasite burdens expressed as LDU with each data point representing
858 an individual mouse in WT (blue) and *miR-132*^{-/-} (*miR-132*^{-/-}; red) mice. Data from 4
859 independent infection experiments.

860 **C.** Mean WT and *miR-132*^{-/-} spleen parasite burdens from the 4 independent
861 experiments shown in (B). Lines link individual experiments.

862 **D.** Splenic parasite burdens relative to WT group (WT mean = 1) for each of the 4
863 experiments shown in (B), with each data point representing individual mouse.

864 **E.** Spleen size expressed as % body weight for d0 (naïve) or day 28 *L. donovani* infected
865 WT (blue) and *miR-132*^{-/-} (*miR-132*^{-/-}; red) mice.

866 **F.** Liver size expressed as % body weight for d0 (naïve) or day 28 *L. donovani* infected
867 WT (blue) and *miR-132*^{-/-} (red) mice.

868 Data information: Significance determined by unpaired t-test, and in (C) by paired t-test
869 of mean values. * p<0.05, ** p<0.01, *** p<0.001, **** p<0.0001.

870

871

872 **EXPANDED VIEW FIGURE LEGENDS**

873

874 **Expanded View Figure EV1: The miR-132/212 cluster regulates RP mRNA levels**
875 **in CD4⁺ T cells from chronically infected spleens.**

876 **A.** Expression of phosphorylated CREB (Ser133), total CREB and β-actin loading
877 control in naïve CD4⁺ T cells cultured for indicated number of hours in presence (+) or
878 absence (-) of anti-CD3 / anti-CD28, as determined by Western blot. Numbers indicate
879 intensity normalised to 1 hour unstimulated samples (lane 1) and corrected by β-actin
880 loading control. Representative of two independent experiments from 3 pooled mice
881 each.

882 **B.** Relative expression of miR-132-3p and miR-212-3p determined by qPCR in naïve
883 mouse CD4⁺ T cells stimulated with anti-CD3/anti-CD28 for 18 hours under Th0 (non-
884 polarising; white), Th1 (rIL-12/anti-IL-4; grey) or Th2 conditions (rIL-4/anti-IFNγ; black)
885 relative to level in naïve cells prior to stimulation.

886 **C.** Fold change of all RP transcripts (grey) in Th2 cells compared to naïve CD4 T cells.
887 Data taken from RNA sequencing experiments described in reference 24. Fold changes
888 in IL-10 (red) and IL-4 (blue) indicated for comparison. The statistical significance of the
889 observed up-regulation of RP transcripts in Th1 cells is determined by Chi-squared test.
890

891 **Expanded View Figure EV2: The B-TFIID cofactor BTAF1 is a direct miR-132 target**
892 **in CD4⁺ T cells.**

893 **A.** Volcano plot of RNAseq gene expression in purified CD62L⁺ CD44⁻ naïve WT cells
894 before and after 1 day (18h) stimulation with anti-CD3/anti-CD28. Fold change
895 determined as log2 mean FPKM (stimulated / pre-stimulation) from 4 WT mice.
896 Transcripts significantly different (p<0.05) shown in red.

897 **B.** Volcano plot of RNAseq gene expression in purified CD62L⁺ CD44⁻ naïve *miR-132*^{-/-}
898 cells before and after 1 day (18h) stimulation with anti-CD3/anti-CD28. Fold change
899 determined as log2 mean FPKM (stimulated / pre-stimulation) from 4 WT mice.
900 Transcripts significantly different (p<0.05) shown in red.

901 **C.** RNAseq gene expression levels of BTAF1 from pre-stimulation (d0), 18h anti-
902 CD3/anti-CD28 (d1) and the spleen of d28 *L. donovani* infection (Ld), from WT (blue)
903 and *miR-132*^{-/-} (red) mice (n=4-5 mice per group). Significance determined by unpaired
904 t-test as indicated.

905 **D.** Schematic of miR-212/132-3p 7mer-m8 site in the 3'UTR of *BTAF1* transcript,
906 showing conservation in human, mouse and chimp. The site is also conserved in, rhesus,
907 squirrel, rabbit, pig, cow, cat, dog, brown bat, elephant, opossum, macaw and chicken;
908 but not rat or lizard.

909 **E.** Relative luciferase activity in mouse 3T3 cells transfected with plasmid containing
910 WT (white) or miR-212/132-mutant (grey) *BTAF1* 3'UTR immediately downstream of
911 renilla luciferase, in the presence of miR-132-3p or miR-212-3p mimics. Error bars
912 indicate SEM from eight replicate treatments. Significance determined by unpaired t-
913 test.

914 **F.** Nucleotide sequences of mouse mature miRNA derived from miR-212/132 cluster.
915 Seed sequences indicated in bold.

916 **G.** Volcano plots of RNAseq gene expression for transcripts containing a poorly
917 conserved miR-132-5p site (upper panels) or a broadly evolutionary conserved miR-
918 212-5p site (lower panels). Fold change determined as log2 mean FPKM *miR-132*^{-/-}
919 /WT) from 4 WT and *miR-132*^{-/-} mice. Transcripts significantly different between WT and
920 *miR-132*^{-/-} (p<0.05) shown in red. Data compares pre-stimulation naïve CD4 T cells (d0,

921 left panels); after 18h *in vitro* stimulation with anti-CD3/anti-CD28 (d1, middle panels);
922 and from the spleens of d28 *L. donovani*-infected mice. Transcripts that are significantly
923 different ($p < 0.05$) and show >2 fold change in expression are indicated.

924 **H.** RNA levels of BACH2 (based on RNA-seq) from pre-stimulation (d0), 18h anti-
925 CD3/anti-CD28 (d1) and the spleen of d28 *L. donovani* infection (Ld), from WT (blue)
926 and *miR-132*^{-/-} (red) mice. Significance determined by unpaired t-test as indicated (n =
927 4-5 mice per group).

928 **I.** Log2 fold change (LFC) in RP genes after 18 hours *in vitro* stimulation of WT (blue)
929 or *miR-132*^{-/-} naïve CD4⁺ T cells with anti-CD3/anti-CD28. Percentages of up-regulated
930 and down-regulated transcripts in WT (40%) and *miR-132*^{-/-} (61%) cells are shown.
931 Statistical significance is determined with Chi-squared test.

932 **J)** DeltaLFC ($\text{LFC}^{\text{miR-132}^{-/-}} - \text{LFC}^{\text{WT}}$) after 18 hours *in vitro* stimulation of WT (blue) or *miR*-
933 *132*^{-/-} naïve CD4⁺ T cells with anti-CD3/anti-CD28. Significance is determined with Chi-
934 squared test. **Data information:** * $p < 0.05$, ** $p < 0.01$.

935

936

937 **Expanded View Figure EV3: miR-132 and its targets p300 and BTAF1 control RP**
938 **expression.**

939 **A.** mRNA levels of indicated RP transcripts determined by qRT-PCR in MEFs transfected
940 with NTC mimics (white) or miR-212-3p mimics (grey). Cultures performed in triplicate.
941 Statistical significance determined by t-test.

942 **B.** Protein levels determined by western blot of RPL27 and RPS10 in MEFs transfected
943 with NTC, miR-132-3p, or miR-212-3p mimics for 48h.

944 **C.** Top enriched molecular function GO terms for miR-132/212-3p predicted target
945 genes. Predictions retrieved from Targetscan, total context score < -0.1 .

946 **D.** Protein levels determined by western blot of BTAF1 and p300 in EL4 cells transfected
947 with NTC, miR-132-3p, or miR-212-3p mimics for 48h.

948 **Data information:** * $p < 0.05$, ** $p < 0.01$.

949

950 **Expanded View Figure EV4: miR-132 controls the balance between IL-10 and IFN γ**
951 **production in CD4 $^{+}$ T cells.**

952 **A.** Intracellular cytokine staining of WT or *miR-132* $^{-/-}$ splenic live CD45.2 $^{+}$ TCR β $^{+}$ CD4 $^{+}$
953 cells for IFN γ and IL-10 from d0 naïve and day 28 *L. donovani* infected mice following
954 *ex vivo* stimulation (4hrs) with PMA and ionomycin.

955 **B.** Antigen-specific IFN γ and IL-10 production by splenic CD4 $^{+}$ T cells from CD45.2 $^{+}$ *L.*
956 *donovani*-infected WT (blue) or *miR-132* $^{-/-}$ (red) mice was assessed as described in
957 materials and methods. Cells were cultured for 3 days in the absence of exogenous
958 stimulation (“Neg”, open circles) or with parasite antigen (“Ag”, closed circles), after
959 which cytokine production by CD4 $^{+}$ T cells from infected (“CD45.2”) or naïve mice
960 (“CD45.1”) was determined. Representative FACS plots for antigen-stimulated CD45.2 $^{+}$
961 cells are shown. Significance determined by unpaired t-test, purified CD4 $^{+}$ T cells from
962 4-5 mice per group.

963

964 **Expanded View Figure 5: miR-132 promotes protective immunity to *L. donovani*.**

965 **A.** Percentage of IL10 $^{+}$ splenic live CD45.2 $^{+}$ TCR β $^{+}$ CD4 $^{+}$ cells for IL-10 in d0 naïve and
966 d21 in *L. donovani*-infected WT (blue), *IL-10* $^{+/-}$ (open green) and *IL-10* $^{-/-}$ (filled green)
967 mice. d21 used due to accelerated parasite clearance and immune resolution in *IL-10* $^{-/-}$
968 mice. Significance determined by ANOVA compared to WT group (n=3-5 per group).

969 **B.** Percentage of IFN γ $^{+}$ splenic live CD45.2 $^{+}$ TCR β $^{+}$ CD4 $^{+}$ cells for IL-10 in d0 naïve and
970 d21 in *L. donovani*-infected WT (blue), *IL-10* $^{+/-}$ (open green) and *IL-10* $^{-/-}$ (filled green)
971 mice. d21 used due to accelerated parasite clearance and immune resolution in *IL-10* $^{-/-}$
972 mice. Significance determined by ANOVA compared to WT group.

973 **C.** Gating strategy for defining distinct myeloid populations in infected mice shown in C.

974 NBNT = non-B non-T i.e. B220 $^{-}$ CD3 $^{-}$ in d0 naïve and d28 infected WT mice.

975 **D.** Total spleen cell numbers or of indicated myeloid populations in d0 naïve and d28
976 *Ld*-infected WT (blue) or *miR-132*^{-/-} (red) mice. Myeloid cells gated as live CD45.2⁺ CD3⁻
977 B220⁻ Ly6G⁻ SS^{lo} singlets then; DC (CD11c⁺ F4/80⁻ MHCII⁺); MφA (CD11b⁺ F4/80⁺
978 CD11c⁻); MφB (CD11c⁺ F4/80⁺ CD11b^{lo}); and MφC (CD11c⁺ F4/80⁺ CD11b^{hi}). Bars
979 show mean + SEM. Data pooled from two independent experiments (n=4-5 per group
980 for each experiment). Significance determined by unpaired t-test as indicated.

981 **E.** Total spleen cell numbers or of indicated myeloid populations in d0 naïve and d21
982 *Ld*-infected WT (blue), *IL-10*^{+/-} (open green) and *IL-10*^{-/-} (filled green) mice (n=3-5 per
983 group). Myeloid cells gated as in (**D**). Bars show SEM. Significance determined by one-
984 way ANOVA and is shown compared to WT group.

985 **F.** Spontaneous and LPS-induced IL-10 production by indicated spleen myeloid
986 populations (as in **D**) from N (naïve) and *Ld*-infected mice (d28), determined by
987 intracellular cytokine staining. n.d. not detected i.e. cell type absent in naïve mice.
988 Significance determined by unpaired t-test as indicated, and data pooled from 2
989 independent experiments each with 3-5 mice per group. Bars show mean + SEM

990 **G.** Day 21 liver parasite burdens expressed as LDU (Leishman Donovan units) in WT
991 (blue) and *miR-132*^{-/-} (red) mice. Each data point represents an individual mouse.
992 Significance determined by unpaired t-test

993 **H.** Left hand panel: Day 28 liver parasite burdens expressed as LDU (Leishman
994 Donovan units) in WT (blue) and *miR-132*^{-/-} (red) mice. Right hand panel shows same
995 data expressed relative to WT levels (WT mean = 1). Data from 4 independent infection
996 experiments with 4-5 mice per group per experiment. Significance determined by
997 unpaired t-test.

998 **I.** Day 42 liver parasite burdens expressed as LDU (Leishman Donovan units) in WT
999 (blue) and *miR-132*^{-/-} (red) mice. Each data point represents an individual mouse.
1000 Significance determined by unpaired t-test.

1001 **J.** Spleen size expressed as % body weight for naïve (= 0 parasite dose) or day
1002 28 *L. donovani* infected WT (blue) and *miR-132*^{-/-} (red) mice. Mice were infected with 10,

1003 30 or 100×10^6 *L. donovani* amastigotes. Data pooled from 2 independent experiments
1004 with 3-5 mice per group. Significance determined by unpaired t-test.

1005

1006 **K.** Liver size expressed as % body weight for naïve (= 0 parasite dose) or day 28 *L.*
1007 *donovani* infected WT (blue) and *miR-132*^{-/-} (red) mice. Mice were infected with 10, 30
1008 or 100×10^6 *L. donovani* amastigotes. Data pooled from 2 independent experiments with
1009 3-5 mice per group. Significance determined by unpaired t-test. Boxes for (J-K) extend
1010 from 25-75th percentile, whiskers are minimum and maximum values, and horizontal
1011 lines indicate median

1012 Data information: * $p < 0.05$, ** $p < 0.01$, *** $p < 0.001$, **** $p < 0.0001$.

1013

Fig. 1

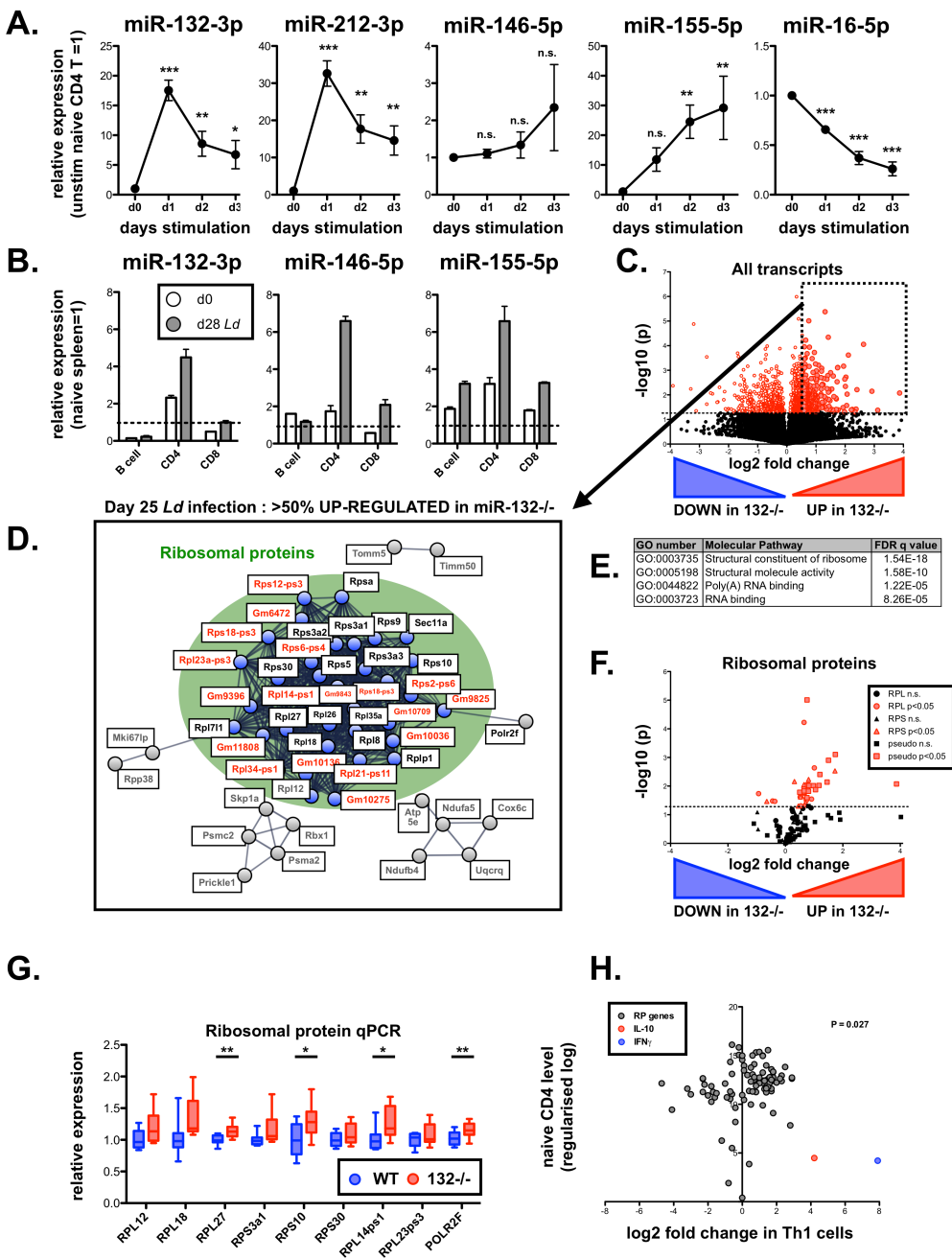


Fig. 2

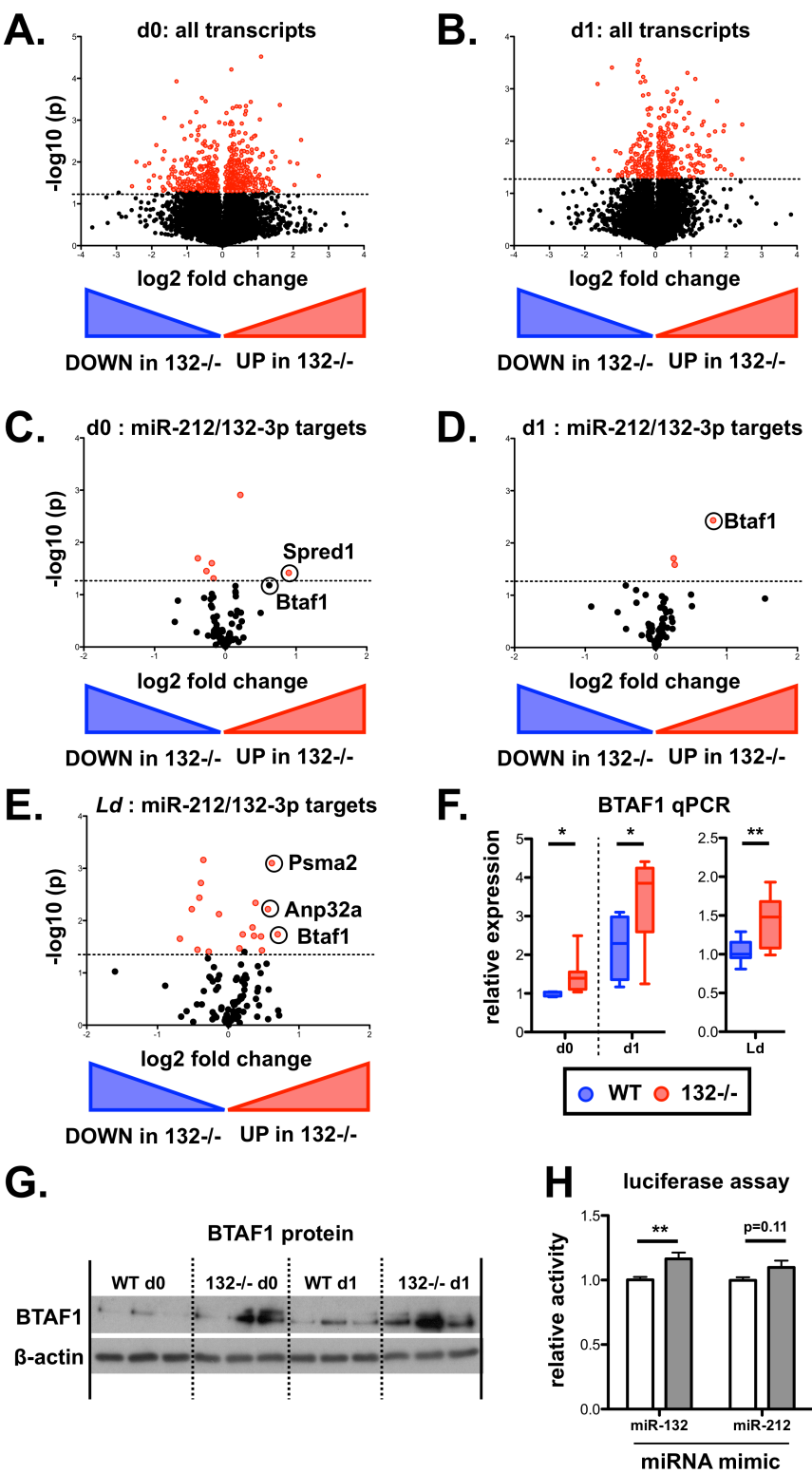
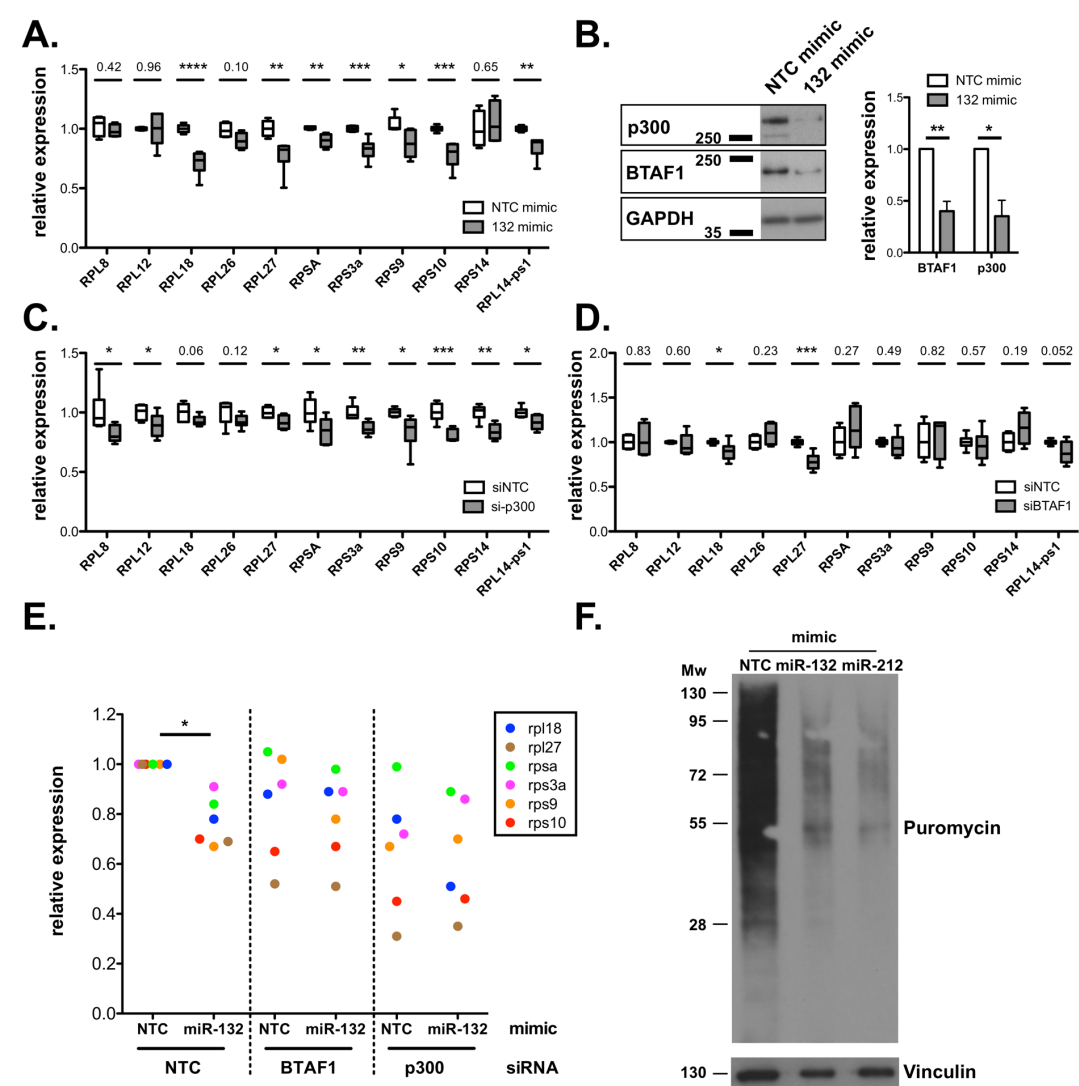
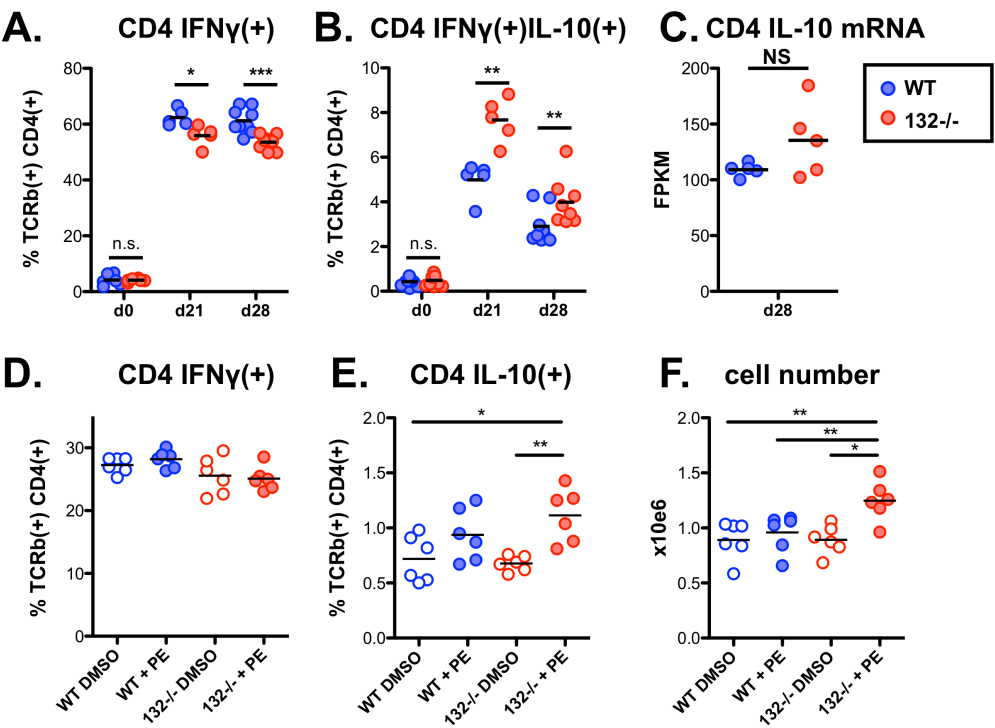


Fig. 3



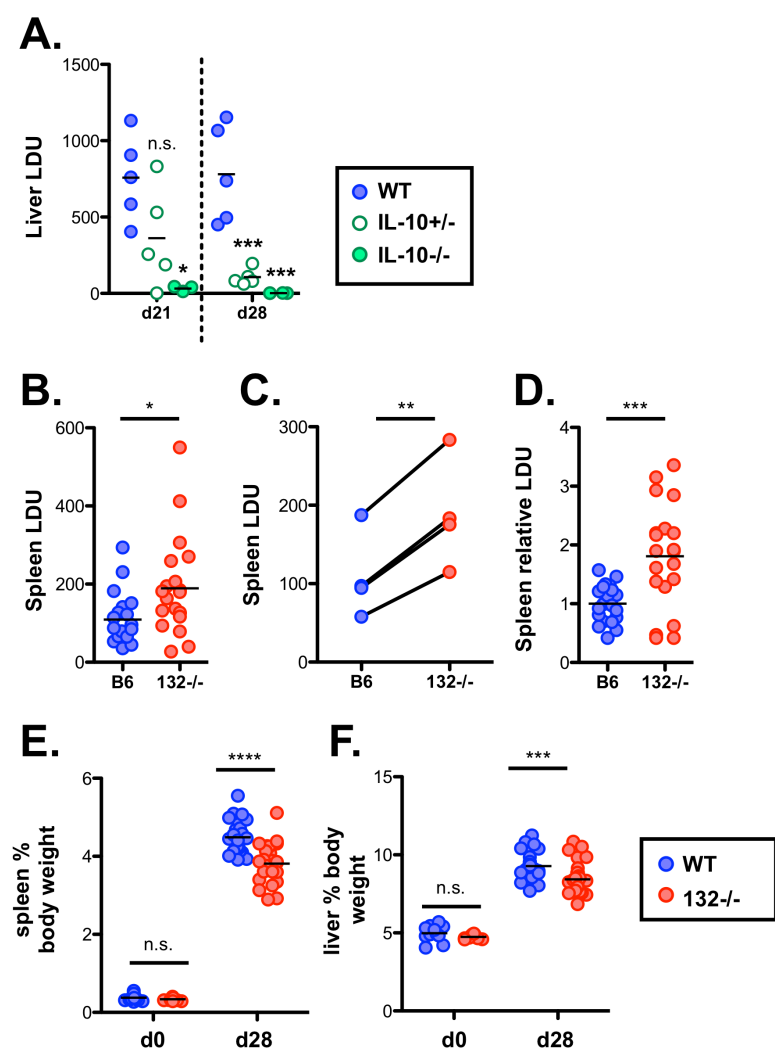
1016

Fig. 4



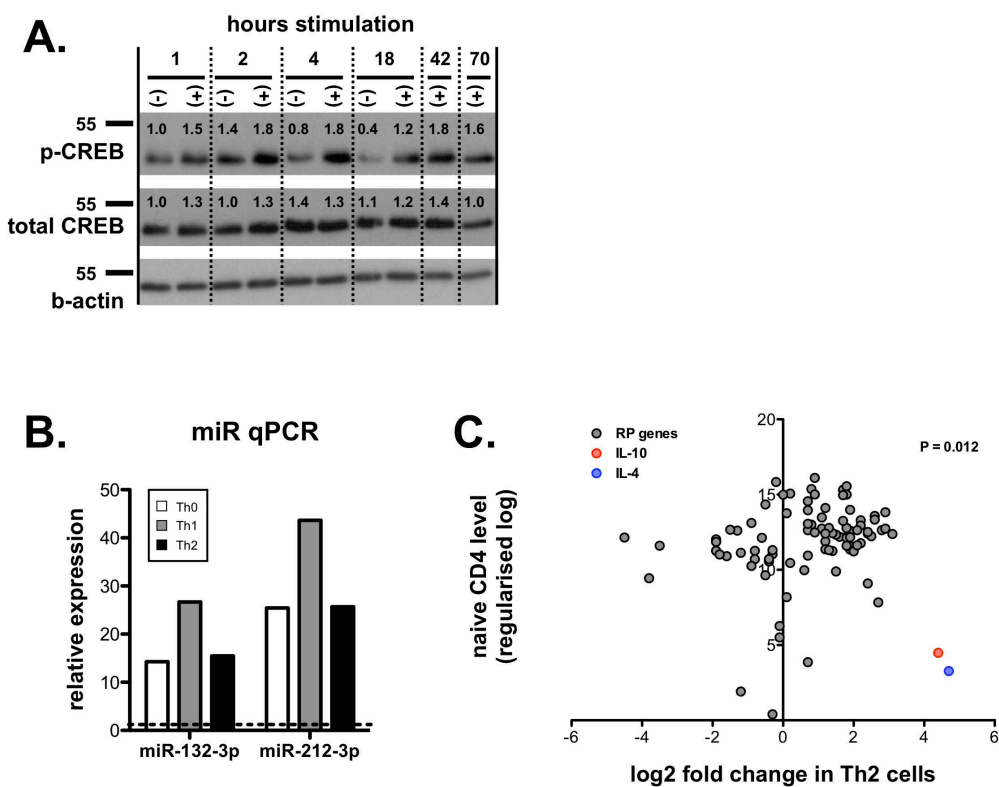
1017

Fig. 5



1018

Fig. EV1



1019

Fig. EV2

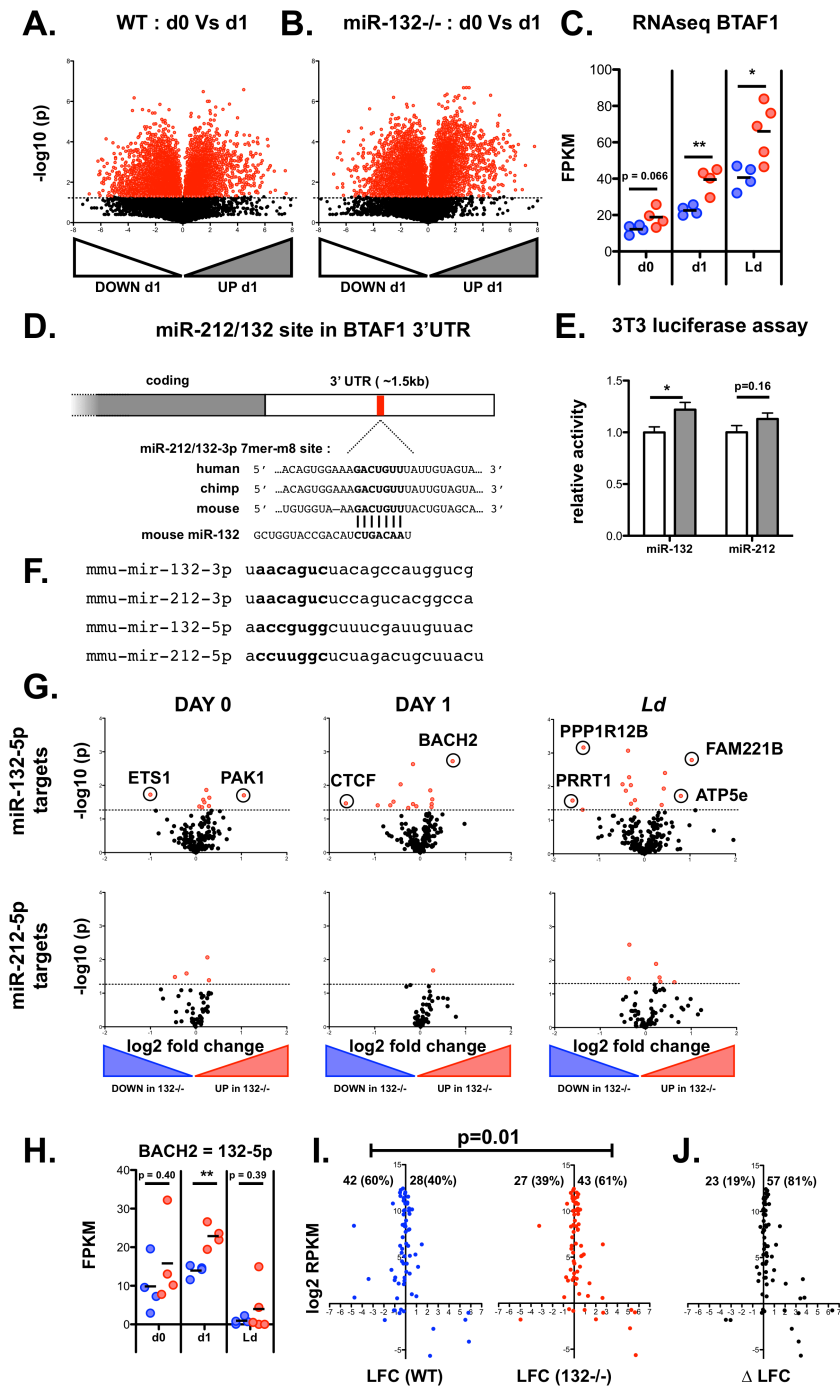
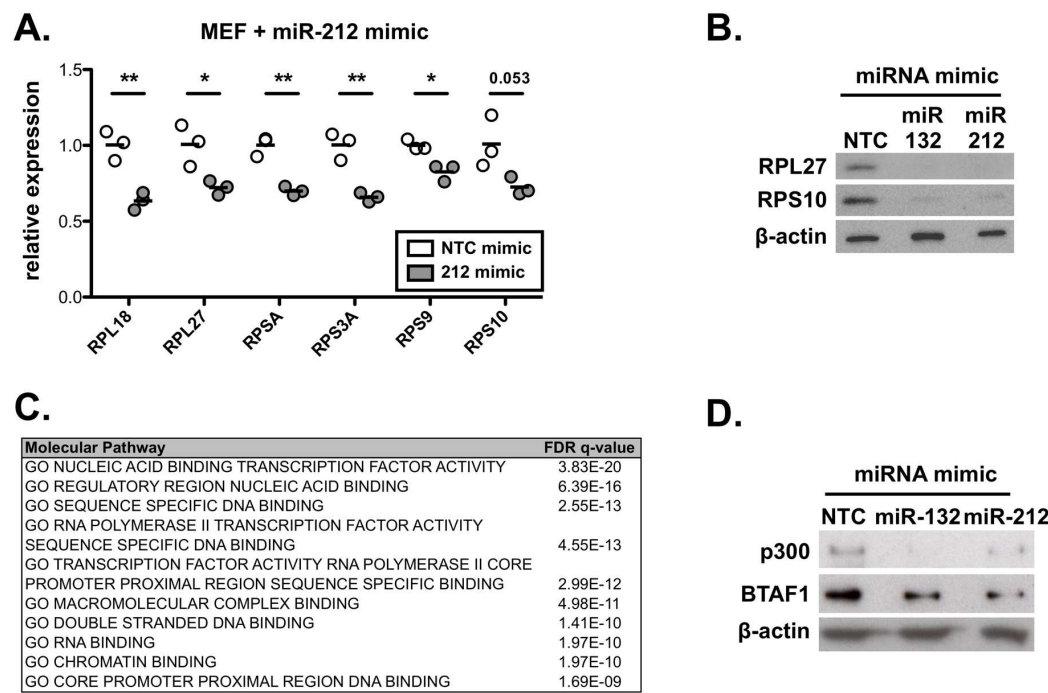


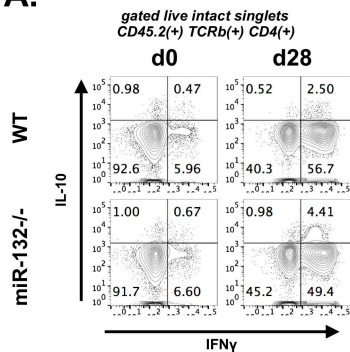
Fig. EV3



1021

Fig. EV4

A.



B.

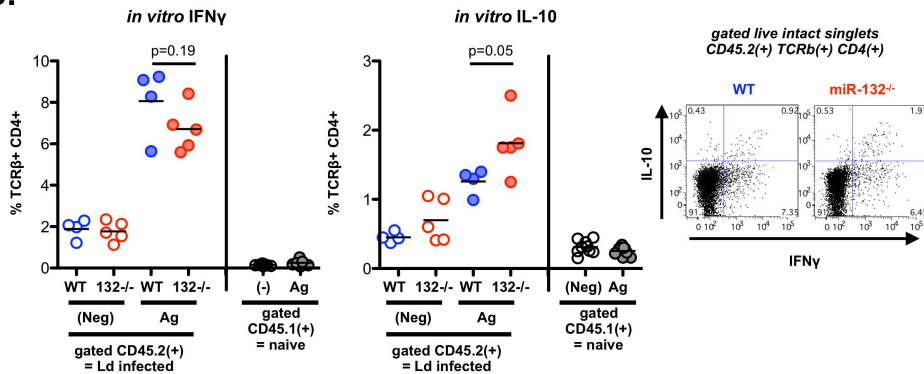
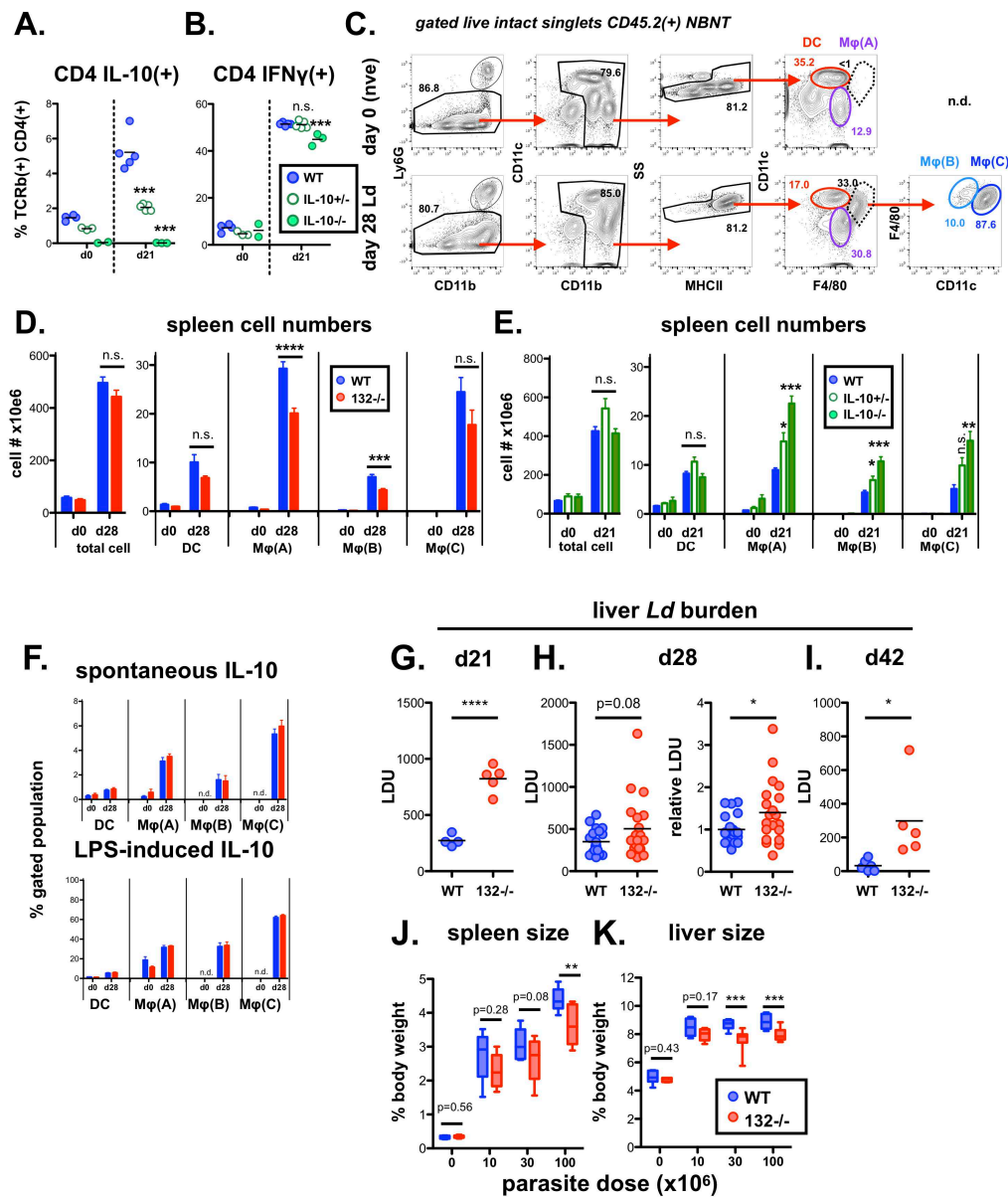


Fig. EV5



1023

1024